Proceedings of the International Conference on Creationism

Volume 9
Print Reference: 540-560

Article 5

2023

Radiohalos Through Earth History – What Clues Can They Provide Us?

Andrew A. Snelling
Answers in Genesis

Recommended Citation
Snelling, Andrew A. (2023) "Radiohalos Through Earth History – What Clues Can They Provide Us?," *Proceedings of the International Conference on Creationism*: Vol. 9, Article 5.
DOI: 10.15385/jpicc.2023.9.1.28
Available at: https://digitalcommons.cedarville.edu/icc_proceedings/vol9/iss1/5

Snelling, A.A. 2023. Radiohalos through earth history–What clues can they provide us? In J.H. Whitmore (editor), *Proceedings of the Ninth International Conference on Creationism*, pp. 540-560. Cedarville, Ohio: Cedarville University International Conference on Creationism.

RADIOHALOS THROUGH EARTH HISTORY– WHAT CLUES CAN THEY PROVIDE US?

Andrew A. Snelling, Answers in Genesis, PO Box 510, Hebron, KY 41048, asnelling@answersingenesis.org.

ABSTRACT

Radiohalos are a physical record of radioactive decay that occurred in granites and metamorphic rocks through earth history. They result from damage to the host crystals, primarily biotite, by α-particles produced in the ^{238}U decay chain within tiny zircon inclusions. However, radiohalos are annealed at 150°C, so those observed today even in Precambrian rocks are likely only due to accelerated ^{238}U decay and associated hydrothermal fluid activity during the Flood. There may not have been any major magmatic events producing hydrothermal fluids capable of forming radiohalos between the unique conditions during the Creation Week and the upheavals of the Flood cataclysm. Therefore, Precambrian granites and metamorphic rocks then affected by the Flood would have generated new radiohalos as they cooled below that temperature. The radiohalos data was selected for 147 granites and regional metamorphic rocks spanning the conventional geologic timescale from 33-3200 Ma whose samples had followed a protocol of similar numbers of slides scanned for radiohalos per sample averaged accordingly to provide statistically robust comparisons between rock units. The plotted radiohalos frequency data were interpreted as consistent with the pre-Flood/Flood boundary being approximately at the Precambrian/Cambrian boundary in the rock record. However, they are unable to distinguish the location of the Flood/post-Flood boundary, as 100 million years' worth of accelerated ^{238}U decay (at today's measured rate) are needed to generate good visible radiohalos. Three small peaks in the radiohalos frequencies in Precambrian granites and metamorphic rocks may coincide with accelerated tectonic activity of God's supernatural creative work on Days 1, 2 and 3 of the Creation Week. The highest peak in the radiohalos frequency data in the first half of the Phanerozoic coincides with the formation of granites and metamorphic rocks during the catastrophic plate tectonics of the Flood. Some of the highest radiohalos numbers are in granites associated with hydrothermal metallic ore veins consistent with the highest radiohalos numbers being indicative of hydrothermal fluid activity. The reason that there are relatively higher radiohalos numbers in some Precambrian metamorphic rocks compared to the Precambrian granites may be due to more biotite grains being in those rocks facilitating the generation of many new radiohalos during the Flood as heat from accelerated ^{238}U decay activated water more easily permeating those biotite flakes. Further data may enhance and/or add to these conclusions, although it is unlikely that they will be significantly changed.

KEYWORDS

radiohalos, granites, metamorphic rocks, accelerated decay, annealing, pre-Flood, Flood, post-Flood

I. INTRODUCTION

Radiohalos (abbreviated from radioactive halos) are minute circular zones of darkening (39-70 μm in diameter) surrounding tiny central mineral inclusions or crystals within some minerals. Often concentric darkened rings are distinguishable within the darkened circular areas. While radiohalos appear in fluorite, cordierite, quartz, and to a lesser extent K-feldspars, they are best observed in thin microscope sections of the black mica, biotite, where the tiny inclusions (or radiocenters) are usually zircon crystals. The significance of radiohalos is due to them being a physical, integral historical record of the decay of radioisotopes in the radiocenters over a period of time. First reported between 1880 and 1890, their origin was a mystery until the discovery of radioactivity. Then in 1907 Joly (1907) and Mügge (1907) independently suggested that the darkening of the minerals around the central inclusions is due to the alpha (α) particles produced by α-decays in the radiocenters. These α-particles are "fired" in all directions like "bullets" and thus damage the crystal structure of the surrounding minerals. It is known as Frenkel defect (a type of point defect) accumulation in which smaller atoms are dislodged from their places in the crystal lattice creating vacancies while they accumulate interstitially. This process produces concentric shells of darkening of discoloration (Fig. 1). When observed in thin sections these shells are concentric circles with diameters between 10 and 40 μm, simply representing planar sections through the concentric spheres centered around the inclusions (Gentry 1973).

Many years of subsequent investigations have established that the radii of the concentric circles of the radiohalos as observed in thin sections are related to the α-decay energies. This enables the radioisotopes responsible for the α-decays to be identified (Gentry 1974, 1984, 1986, 1988; Snelling 2000b). Most importantly, when the central inclusions, or radiocenters, are very small (about 1 μm)

the radiocenters around them have been unequivocally demonstrated to be products of the α-emitting members of the ^{238}U decay series to stable ^{206}Pb, and occasionally the ^{232}Th decay series to stable ^{208}Pb. It has been demonstrated that the radii of these rings correspond to the energies of specific α-particles in the ^{238}U decay series and their travel ranges (Gentry 1984). Thus, a fully-developed ^{238}U radiohalo should have eight visible concentric rings which correspond to the eight α-decay steps in the ^{238}U decay series. It has also been determined that such a halo requires between 500 million and 1 billion α-decays to be fully-developed and darkened (Fig. 1) (Gentry 1988). The radii of the concentric multiple spheres, or rings in thin sections, correspond to the ranges in the host minerals of the α-particles from the α-emitting radioisotopes in the ^{238}U and ^{232}Th decay series (Gentry 1973, 1974, 1984) (Fig. 2). ^{235}U radiohalos have not been observed. This is readily accounted for by the scarcity of ^{235}U (only 0.7% of the naturally-occurring U), since large concentrations of the parent radionuclides are needed to produce the concentric ring structures of the radiohalos.

Ordinary radiohalos can be defined, therefore, as those that are initiated by ^{238}U or ^{232}Th α-decay, irrespective of whether the actual halo sizes closely match the respective idealized patterns (Fig. 2). In many instances the match is very good, the observed sizes agreeing very well with the ^{4}He ion penetration ranges produced in biotite, fluorite, and cordierite (Gentry 1973, 1974). U and Th radiohalos usually are found in igneous rocks, most commonly in granitic rocks and in granitic pegmatites. While U and Th radiohalos have been found in over 40 minerals, their distribution within these minerals is very erratic (Ramdohr 1933, 1957, 1960; Stark 1936). Thus far there have been no hypotheses proposed to explain the cause(s) of this erratic distribution. Radiohalos have even been found in diamonds (Gentry 1998; Armitage and Snelling 2008; Schulze and Nasdala 2017). Biotite is quite clearly the major mineral in which U and Th radiohalos occur (Bower et al. 2016a, b). Wherever found in ubiquitous large (1-5 mm in diameter) biotite flakes the radiohalos are prolific, and are associated with tiny (1-5 μm in diameter) U-bearing zircon grains or Th-bearing monazite grains as the radiocenters. The ease of thin section preparation, and the clarity of the radiohalos in these sections, have made biotite an ideal choice for numerous radiohalo investigations, namely, those of Joly (1917a, b, 1923, 1924), Lingen (1926), Iimori and Yoshimura (1926), Kerr-Lawson (1927, 1928), Wiman (1930), Henderson and Bateson (1934), Henderson and Turnbull (1934), Henderson et al. (1934), Henderson and Sparks (1939), Gentry (1968, 1970, 1971), Snelling and Armitage (2003), and Snelling (2005a). U, Th, and other specific halo types in most of these studies have been observed mainly in Precambrian rocks, so much remains to be learned about their occurrence in rocks from the other geological periods of the strata record. However, some studies have shown that they do exist in rocks stretching from the Precambrian to the Tertiary (Holmes 1931; Stark 1936; Wise 1989; Snelling and Armitage 2003; Snelling 2005a). Unfortunately, in some of those published studies the radiohalo types were not specifically identified.

Some unusual radiohalo types that appear to be distinct from those formed by ^{238}U and/or ^{232}Th α-decay have been observed (Gentry 1970, 1971, 1973, 1984, 1986; Gentry et al., 1973, 1976a, 1978; Snelling, 2000b). Of these, only the Po (polonium) radiohalos can presently be identified with known α-radioactivity (Gentry 1967, 1968, 1973, 1974; Gentry et al. 1973, 1974). There are three Po isotopes in the ^{238}U-decay chain. In sequence they are ^{218}Po (half-life of 3.1 minutes), ^{214}Po (half-life of 164 microseconds), and ^{210}Po (half-life of 138 days). Po radiohalos contain only three rings, two rings or the one ring produced by these three Po α-emitters respectively (Fig. 3). They are designated by the first (or only) Po α-emitter in the portion of the decay sequence that is represented. The presence in Po radiohalos of only the rings of the three Po α-emitters

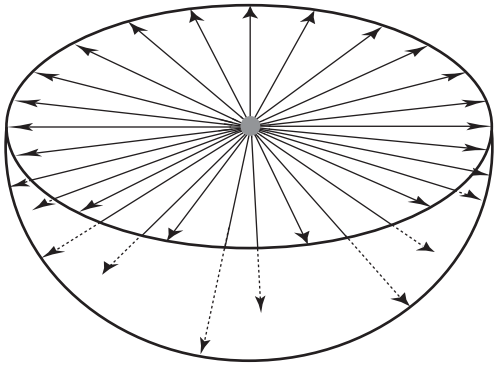

Figure 1. Sunburst effect of alpha-damage trails. The sunburst pattern of α-damage trails produces a spherically colored shell around the halo center. Each arrow represents approximately 5 million α-particles emitted from the center. Halo coloration initially develops after about 100 million α-decays, becomes darker after about 500 million, and very dark after about 1 billion (after Gentry 1988).

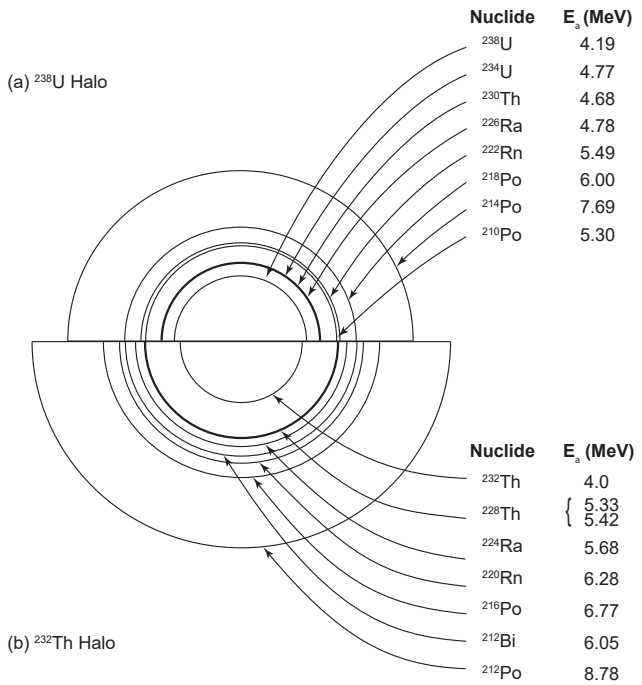

Figure 2. Schematic drawing of (a) a ^{238}U halo, and (b) a ^{232}Th halo, with radii proportional to the ranges of α-particles in air. The nuclides responsible for the α-particles and their energies are listed for the different halo rings (after Gentry 1973).

implies that the radiocenters which produced these Po radiohalos initially contained only either the respective Po radioisotopes that then parented the subsequent α-decays, or a non-α-emitting parent (Gentry 1971; Gentry et al. 1973). These three Po radiohalo types occur in biotite from granitic rocks (Gentry 1968, 1971, 1973, 1974, 1984, 1986, 1988; Gentry et al. 1973, 1974; Wise 1989; Snelling and Armitage 2003; Snelling 2005a).

Joly (1917b, 1924) was probably the first to investigate ^{210}Po radiohalos and was clearly baffled by them. Because Schilling (1926) saw Po radiohalos located only along cleavages and cracks in fluorite from Wölsendorf in Germany, he suggested that they originated from preferential deposition from secondary fluid transport of Po in U-bearing solutions. Henderson (1939) and Henderson and Sparks (1939) invoked a similar but more quantitative hypothesis to explain Po radiohalos along conduits in biotite. However, those Po radiohalos found occurring along much more restricted cleavage planes, similar to those found by Gentry (1973, 1974), have been more difficult to account for. The reason given for these attempts to account for the origin and formation of the Po radiohalos by some secondary process is simple – the half-lifes of the respective Po isotopes are far too short to be reconciled with the Po having been primary, that is, originally in the granitic magmas which are usually claimed to have slowly cooled to form the granitic rocks that now contain the Po-radiohalo-bearing biotite grains. The half-life of ^{218}Po, for example, is 3.1 minutes. However, this is not the only formidable obstacle for any secondary process that transported the Po into the biotite as, or after, the granitic rocks cooled. First, there is the need for the isotopic separation of the Po isotopes, or their α-decay precursors, from their parent ^{238}U having occurred naturally (Gentry et al. 1973). Second, the radiocenters of very dark ^{218}Po radiohalos, for example, may need to have contained as much as 5 x 10^9 atoms (a concentration of greater than 50%) of ^{218}Po (Gentry 1974), yet the host minerals contain only ppm abundances of ^{238}U, which apparently means only a negligible supply of ^{218}Po daughter atoms is available for capture in a radiocenter at any given time. But these ^{218}Po atoms must also migrate or diffuse from their source at very low diffusion rates through surrounding mineral grains to be captured by the radiocenters before the ^{218}Po decays (Fremlin 1975; Gentry 1968, 1975).

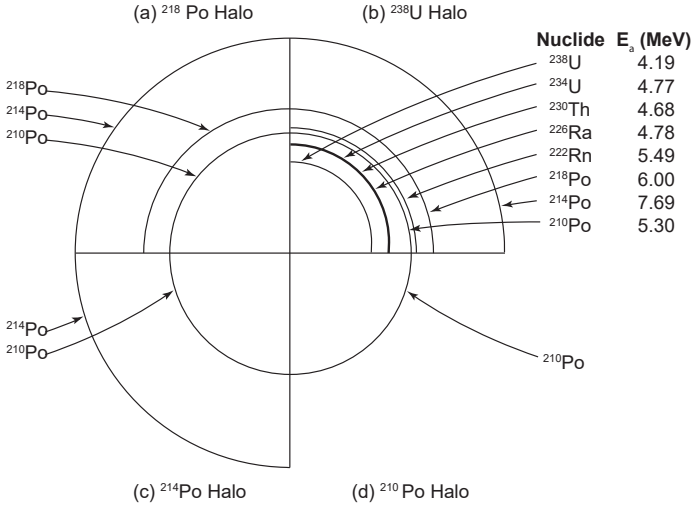

Figure 3. Composite schematic drawing of (a) a ^{218}Po halo, (b) a ^{238}U halo, (c) a ^{214}Po halo, and (d) a ^{210}Po halo with radii proportional to the ranges of α-particles in air. The nuclides responsible for the α-particles and their energies are listed for the different halo rings (after Gentry 1973).

Therefore, there are strict time limits for the formation of the Po radiohalos by primary or secondary processes in granites. Studies of some Po radiohalo centers in biotite (and fluorite) have shown little or no U in conjunction with anomalously high ^{206}Pb/^{207}Pb and/or Pb/U ratios, which would be expected from the decay of Po without the U precursor that normally occurs in U radiohalo centers (Gentry 1974; Gentry et al. 1974). Indeed, many ^{206}Pb/^{207}Pb ratios were greater than 21.8 reflecting a seemingly abnormal mixture of Pb isotopes derived from Po decay independent of the normal U-decay chains (Gentry 1971; Gentry et al. 1973). Thus, based on these data, Gentry advanced the hypothesis that the three different types of Po radiohalos in biotite represent the decay of primordial Po (that is, original Po not derived by ^{238}U-decay), and that the rocks hosting these radiohalos must be primordial rocks produced by fiat creation, given that the half-life of ^{214}Po is only 164 microseconds (Gentry 1979, 1980, 1982, 1983, 1984, 1986, 1988, 1989). He thus perceived that all granites must be Precambrian, and part of the earth's crust created during the Creation Week.

As a consequence of Gentry's creation hypothesis, the origin of the Po radiohalos has remained controversial and thus apparently unresolved. Of the 22 locations then known where the rocks contained Po radiohalos, Wise (1989) had determined that six of the locations hosted Phanerozoic granitic rocks that intruded fossiliferous (and thus Flood-deposited) sedimentary strata, a large enough proportion to severely question Gentry's hypothesis of primordial Po in fiat created granitic rocks. Many of these Po radiohalo occurrences are also in proximity to higher than normal U concentrations in nearby rocks and/or minerals, suggesting ideal sources for fluid separation and transport of the Po. Subsequently, Snelling (2000b) reviewed the literature on radiohalos. He thoroughly discussed the many arguments and evidences used in the debate that had ensued over the previous two decades, and concluded that there were insufficient data on the geological occurrence and distribution of the Po radiohalos for the debate to be decisively resolved. He then recognized the spatial association of Po radiohalos to ^{238}U radiohalos meant that the Po which parented the adjacent Po radiohalos may have been derived from the ^{238}U decay products in the radiocenters of the ^{238}U radiohalos. He also observed that many radiohalo-hosting biotite flakes had been hydrothermally altered. Furthermore, many of the host Phanerozoic granites had intruded into fossil-bearing sedimentary layers that therefore were deposited during the Flood. Thus, those and other granites intruded into fossil-bearing, Flood-deposited sedimentary layers had to form during the Flood subsequent to the deposition of those sedimentary layers and could not be creation rocks as postulated by Gentry (1988). Of course, this does not preclude many Precambrian granites having been created during the Creation Week.

Furthermore, Snelling (2000b) found that there are now significant reports of ^{210}Po as a detectable species in volcanic gases, in volcanic/hydrothermal fluids associated with subaerial volcanoes

and fumeroles, and associated with mid-ocean ridge hydrothermal vents and chimney deposits (Hussain et al. 1995; LeCloarec et al. 1994; Rubin 1997), as well as in ground waters (Harada et al. 1989; LaRock et al. 1996). The distances involved in this fluid transport of the Po are several kilometers (and more), so there is increasing evidence of the potential viability of the secondary transport of Po by hydrothermal fluids during pluton emplacement, perhaps in the waning stages of the crystallization and cooling of granitic magmas (Snelling and Woodmorappe 1998; Snelling 2000b, 2008a).

Consequently, Snelling and Armitage (2003) investigated the Po radiohalo occurrences in three Phanerozoic granitic plutons and logically argued for a model of Po radiohalo formation involving secondary transport of Po by hydrothermal fluids during crystallization and cooling of the granitic magmas. Their data and details of this hydrothermal fluid transport model were initially published by Snelling et al. (2003), but full details encompassing these results were elaborated upon in Snelling (2005a). He proposed that hydrothermal fluids infiltrating along the cleavage planes within biotite flakes dissolved ^{226}Ra, ^{222}Rn and the Po isotopes emanating from ^{238}U decay within the zircon radiocenters of the ^{238}U radiohalos. At conducive sites down flow within the same biotite flakes the Po isotopes were deposited and concentrated in what became the radiocenters for ^{218}Po, ^{214}Po and ^{210}Po radiohalos as the Po isotopes decayed. Hydrothermal fluids are typically Cl-rich and are known to be capable of dissolving ^{226}Ra, ^{222}Rn and the Po isotopes, the latter particularly bonding with Cl (Bagnall 1957). Hydrothermal fluids also carry S, and because Po behaves geochemically the same as Pb it also bonds with S (Bagnall 1957). Furthermore, the mica sheets making up the biotite structure are weakly bonded by K, OH, and F ions, so S and Cl ions can occasionally substitute at point loci within the cleavage planes. It was thus postulated by Snelling (2005a) that as the hydrothermal fluids carrying ^{222}Rn and the Po along the cleavage planes between the biotite sheets, Po atoms were attracted to those point loci where they decayed, only to be replaced by more Po atoms attracted to the same S or Cl point loci. The Po radiocenters were thus formed surrounded by Po radiohalos.

Whereas Po radiohalos would appear to indicate extremely rapid geological processes were responsible for their production (because of the extremely short half-lifes of the Po isotopes responsible), ^{238}U and ^{232}Th radiohalos appear to be evidence of long periods of radioactive decay, assuming decay rates have been constant at today's rates throughout earth history. Indeed, it has been estimated that dark, fully-formed U and Th radiohalos require around 100 million years' worth of radioactive decay at today's rates to form (Gentry 1973, 1974; Humphreys 2000; Snelling 2000b). Thus, the presence of mature U and Th radiohalos in granitic rocks globally throughout the geological record would indicate that at least 100 million years' worth of radioactive decay at today's rates had occurred during earth history. Therefore, the requirement of grossly accelerated ^{238}U decay is essential to this hydrothermal fluid model for the transport of the Po isotopes from the decay of ^{238}U in the radiocenters of ^{238}U radiohalos (Snelling 2005a). Vardiman et al. (2005) found that the greater the half-life of a radioisotope the greater the decay rate acceleration. Thus, whereas ^{238}U decay would have been grossly accelerated during some past geologically catastrophic event such as the Flood, the very short half-life Po radioisotopes would not have been affected. Several lines of evidence suggest that during the Flood when much of the fossil-bearing sedimentary rock record was accumulating, and when biotite-bearing granites were intruded into those sedimentary rocks, the decay rate of ^{238}U was grossly accelerated (Vardiman et al. 2005). These include systematically-different radioisotope ages for the same rock units dated by multiple methods, helium diffusion in zircons, the quantities of fission tracks matching conventional Phanerozoic stratigraphic ages in tuff beds deposited during the Flood year, and radiocarbon in Phanerozoic coal beds and other organic materials, as elaborated in detail by Vardiman et al. (2005). Thus, whereas today's very slow ^{238}U decay rate produces only a few Ra, Rn and Po atoms very slowly, that grossly accelerated decay rate would have produced huge numbers of Ra, Rn and Po atoms very rapidly, which were then easily transported the short distances within the host biotite flakes to precipitate in the adjacent Po radiocenters and produce the Po radiohalos.

As proposed by Humphreys (2000) and Vardiman et al. (2005), these observable data require that within the Biblical young-earth time framework radioisotope decay therefore had to have been accelerated, but just by how much needs to be determined. If, for example, mature U and Th radiohalos were found in granitic rocks that were demonstrated to have formed during the Flood year, then that would imply at least 100 million years' worth of radioisotope decay at today's rates had occurred at an accelerated rate during the Flood year (Baumgardner 2000; Snelling 2000b, 2005a). Vardiman et al. (2005) postulated the ^{238}U decay rate was accelerated by five orders of magnitude, so it could then be supposed the Po isotopes' decay rates were similarly accelerated, which could make their existence so fleeting there wouldn't be sufficient time for hydrothermal transport to form radiocenters. However, as already noted, Vardiman et al. (2005) also found that the amount of acceleration was related to the present half-lives of the parent radioisotopes, the slower the present decay rate (or the longer the current half-life) resulting in the most acceleration. Thus, with such fast decay rates (short half-lives) today, the Po isotopes would virtually have not been accelerated. Furthermore, the accelerated decay rates would not have resulted in much larger radii for ^{238}U radiohalos, as ring radii are not affected by the decay rates but are related to the energies of the emitted α-particles (Gentry 1973, 1974).

In this hydrothermal model, therefore, the Po accumulated in the radiocenters by time integration as Po atoms were progressively deposited from the passing hydrothermal fluids (Snelling and Armitage 2003; Snelling 2005a). So, instead of the Po radiohalos forming virtually instantaneously as proposed by Gentry (1988), the Po radiohalos formed over hours and days. However, whereas granitic magmas are intruded at 650-730°C, the radiohalos cannot form until the magma has crystallized and the temperature has fallen below 150°C, because above that temperature radiohalos are annealed (Laney and Laughlin 1981). This still has drastic time implications for the formation of granites (Snelling 2008a). Whereas Gentry (1988) concluded that granites were created instantaneously by divine fiat, Snelling (2005a, 2008a, 2014) postulated that granite magmas crystallized and cooled within days, which is still very radical compared to the uniformitarian timescale. Furthermore, if Po

radiohalos were alongside U and Th radiohalos in the same Flood-related granitic rocks, then that would have implications as to the rate of formation and age of these granitic rocks formed during the Flood year within the Biblical timescale.

Subsequently, case studies were undertaken to test this hydrothermal fluid transport model for the formation of Po radiohalos. Most remarkable was the fulfilled prediction of many more Po radiohalos at the staurolite isograd in regionally metamorphosed sandstones in the Great Smoky Mountains, Tennessee-North Carolina, where the metamorphic reaction would have released a lot of water (224 water molecules for every 54 units of muscovite reacting with chlorite; Snelling 2008b). Then, in the Cooma regional metamorphic complex of southeastern Australia the numbers of Po radiohalos increased where water was released in the high-grade zone and in the central granodiorite, but decreased sharply in the zone of partial melting where water was dissolved into the melt, just as expected in the model (Snelling 2008c).

In granites, increased numbers of Po radiohalos were also found where they were predicted to be based on the release of hydrothermal fluids during granite crystallization and cooling (Snelling 2008a). In the Shap Granite of northern England, prolific Po radiohalos matched the higher volume of hydrothermal fluids associated with that granite's large K-feldspar phenocrysts (Snelling 2008d, Glazner and Johnson 2013). The nested plutons of the Tuolumne Intrusive Suite, Yosemite, California (Glazner et al. 2022) contain increasing numbers of Po radiohalos proportional to the increased volumes of active hydrothermal fluids within the sequentially emplaced intrusions (Snelling and Gates 2009). High numbers of Po radiohalos and active hydrothermal fluids coincide with the large K-feldspar phenocrysts in the second to last pluton and the connection to explosive volcanism of the last pluton (Bateman and Chappell 1979; Snelling and Gates 2009; Glazner and Johnson 2013; Glazner et al. 2022). The Bathurst Batholith west of Sydney, Australia, consists of an enormous pluton of 1600 km^2 (620 sq. mi) (the Bathurst Granite) intruded into fossiliferous sedimentary strata and numerous smaller related satellite plutons and dikes, which field and textural data have established were sequentially intruded while still hot (Snelling 2014). The presence of Po radiohalos in all three sequentially-intruded granite phases is evidence that all this intrusive activity, and the cooling of all three granite phases, must have occurred within a week or two so that these Po radiohalos in them formed subsequently within days to weeks. And Snelling (2018) successfully tested the use of Po radiohalos as an exploration guide to locate hydrothermal ore deposits associated with granites, higher numbers of Po radiohalos being spatially associated with hydrothermal ore veins within granites in the New England region of northern New South Wales, Australia.

II. MATERIALS – THE PRESENT STUDY

Radiohalos are thus a physical record of radioactive decay that occurred in granites and metamorphic rocks through earth history. They are the result of damage to the host crystals by α-particles produced in the ^{238}U decay chain (Snelling 2000b). Normally ^{238}U radiohalos are produced. However, there are also radiohalos produced by the three isotopes of Po (^{218}Po, ^{214}Po and ^{210}Po) that are generated towards the end of the ^{238}U decay chain. Because their half-lives are so fleeting (3.1 mins, 164 μsec, and 138 days, respectively), the existence of these Po radiohalos has been "a tiny mystery", though now explained by the hydrothermal fluid transport model proposed and elaborated by Snelling and Armitage (2003) and Snelling (2005a), and tested successively by Snelling (2008b, c, d, 2014, 2018) and Snelling and Gates (2009).

This hydrothermal fluid transport model for the formation of polonium radiohalos involves a pulse of accelerated radioactive decay. Hundreds of millions of years' worth of ^{238}U decay must have occurred within days so enough daughter Po isotopes were produced rapidly to be transported by hydrothermal fluids to closely adjacent locations within the host crystals to form separate ("orphan") Po radiohalos (Snelling 2005a). One major objection raised is the huge amount of heat (as well as radiation) that would seem to be generated by the pulse of accelerated ^{238}U decay. However, Laney and Laughlin (1981) have documented that natural annealing of radiohalos occurs at as low as 150°C. Thus, there may not have been a heat problem because the radiohalos have survived to the present, and/or the radiohalos formed as the host crystals cooled after the heat dissipated from the pulse of accelerated ^{238}U decay. The important corollary to that is the radiohalos we observe today had to form after whatever was the last heating event these rocks suffered.

Because there is abundant evidence that the last pulse of accelerated ^{238}U decay occurred during the Flood, as indicated by the lines of supporting evidences enumerated above (Vardiman et al. 2005), then the radiohalos we observe today had to form during the Flood. That would thus seem to apply not to just the rocks produced by the Flood, but also to the pre-Flood and Creation Week rocks. The latter rocks would have been affected by both the pulse of accelerated ^{238}U decay during the Flood and the heat that pulse produced. It is thus possible that any previously formed radiohalos in Precambrian rocks (if those are pre-Flood and Creation Week rocks) were annealed during the Flood. Yet, there has been insufficient data on the distribution of all radiohalo types in the vast Precambrian geological record. Indeed, the distribution pattern of all radiohalo types in Precambrian granitic and metamorphic rocks might well be significant, providing clues about the earth's early history within the Biblical framework.

Snelling (2005a) made an initial attempt to survey the radiohalos data collected from granites and metamorphic rocks spanning earth history. However, the data he tabulated and plotted were preliminary and insufficient to draw any major conclusions. Yet, it was evident from his data that Precambrian granites generally have fewer radiohalos than Phanerozoic granites. Those Phanerozoic granites were formed during the Flood because they intruded fossiliferous, Flood-deposited sedimentary strata, and they had generated enough water as they crystallized and cooled to produce a lot more radiohalos. In contrast, the Precambrian granites had already been formed, presumably during the Creation Week, as the basement (or foundation) to the Flood rocks and therefore did not necessarily have much water generated in them during the Flood so were thus less able to produce radiohalos. It was also found that certain suitable Precambrian metamorphic rocks have as many radiohalos within them as some Phanerozoic metamorphic rocks. This suggested that whatever the precursor pre-Flood rocks were, some metamorphism of those pre-Flood basement rocks releasing water may have still

occurred during the Flood to generate so many radiohalos.

With this background, it was determined that a fuller study was needed with a lot more radiohalos data to potentially draw better-established conclusions. While there are some radiohalos occurrence data available in the older literature, this study required not just data on where radiohalos are found, but also the quantities of radiohalos at each occurrence. This is so comparisons can be made between rock types at various levels in the geologic record to glean what clues they might provide us regarding radioactive decay in these rock through earth history within the Biblical framework.

III. METHODS

Snelling and Armitage (2003) and Snelling (2005a) devised a method of counting radiohalos for each sample investigated from a designated number of thin sections (usually 50) with approximately 20 biotite flakes per thin section. This allowed for statistical comparisons between samples and rock types. Thus, for this study it was necessary to follow that same procedure to tabulate the needed radiohalos data for rock samples encompassing the geologic record.

Snelling (2005a) had already tabulated radiohalos data for numerous samples, and subsequent studies by Snelling (2008b, c, d, 2014, 2018) and Snelling and Gates (2009) had followed the same procedure. So, all those data were tabulated for this study. Additionally, unpublished, and soon-to-be published, radiohalos data were added to the tabulation in this paper (see below).

Over some years additional samples have been collected, for example, from the granites of northern coastal Queensland, Australia (Bain and Draper 1997; Day et al. 1983), the metamorphic rocks of the Broken Hill region of western New South Wales, Australia (that host the supergiant world-class Broken Hill Ag-Pb-Zn ore deposit) (Stevens and Bradley 2018), and from the granites and metamorphic schists in the Inner Gorge of Grand Canyon, northern Arizona, USA (with the appropriate research and sampling permits from the Grand Canyon National Park) (Ilg et al. 1996; Karlstrom et al. 2003). A few other scattered samples have also been collected on various field trips, as well as samples collected by others and sent in for radiohalos investigation with location documentation, for example, from the granites of the Cornubian Batholith of southwest England (Moscati and Neymark 2020). All rock samples were identically processed to obtain the needed radiohalos data from them, following the method of Snelling and Armitage (2003) and Snelling (2005a).

A standard petrographic thin section was obtained for each sample. In the laboratory, a scalpel and tweezers were used to prize flakes of large, primary biotite loose from the sample surfaces, or where necessary portions of the samples were crushed to liberate the constituent mineral grains. Biotite flakes were then hand-picked and placed on the adhesive surface of a piece of clear Scotch™ tape fixed to a bench surface with its adhesive side up. Once numerous biotite flakes had been mounted on the adhesive surface of this piece of clear Scotch™ tape, a fresh piece of clear Scotch™ tape was placed over them and firmly pressed along its length so as to ensure the two pieces of clear Scotch™ tape were stuck together with the biotite flakes firmly wedged between them. The upper piece of clear Scotch™ tape was then peeled back in order to pull apart the sheets composing the biotite flakes, and this upper piece of clear Scotch™ tape with thin biotite sheets adhering to it was then placed over a standard glass microscope slide so that the adhesive side had the thin mica flakes adhered to it. This procedure was repeated with another piece of clear Scotch™ tape placed over the original Scotch™ tape and biotite flakes affixed to the bench, the adhering biotite flakes being progressively pulled apart and transferred to microscope slides. As necessary, further hand-picked biotite flakes were added to replace those fully pulled apart. In this way tens of microscope slides were prepared for each sample, each with many (at least twenty to thirty) thin biotite flakes mounted on them. This is similar to the method pioneered by Gentry. Fifty microscope slides were prepared for each sample to ensure good representative sampling statistics. Thus, there was a minimum of 1,000 biotite flakes mounted on microscope slides for each sample.

Each thin section for each sample was then carefully examined under a petrological microscope in plane polarized light, and all radiohalos present were identified, noting any relationships between the different radiohalo types (^{238}U, ^{232}Th, ^{218}Po, ^{214}Po, and ^{210}Po). The numbers of each type of radiohalo in each slide were counted by progressively moving the slide backwards and forwards across the field of view, and the numbers recorded for each slide were then tallied and tabulated for each sample. Only radiohalos whose radiocenters were clearly visible were counted. Because of the progressive peeling apart of many of the same biotite flakes during the preparation of the microscope slides due to biotite's perfect basal cleavage, many of the radiohalos appeared on more than one microscope slide, so this procedure ensured each radiohalo was only counted once. The photomicrographs in fig. 4 display some of the typical Po and U radiohalos identified and counted in this and previous studies.

IV. RESULTS

The radiohalos counted for all samples are tabulated in Table 1 (granites) and Table 2 (regional metamorphic rocks). Each table provides the name (where available) of the granite or metamorphic rock, the location of the collected sample(s) and the known or approximate conventional age of the rock unit. It was assumed for the purposes of this study that the conventional ages were valid within the conventional paradigm, but they are used here only to identify the relative positions of the rock units in the geologic record (see the discussion below). Notice also that the rock units are not designated in the tables according to where they fit in the biblical framework of earth history, namely, pre-Flood, Flood, or post-Flood. Instead, it was decided to see if the radiohalos data would differentiate those designations for the studied rock units.

Also included in the tables are the number of samples studied for each rock unit and thus the number of slides (thin sections) that were prepared. Subsequent columns list the counted ^{210}Po, ^{214}Po, ^{218}Po, ^{238}U and ^{232}Th radiohalos. The figures in the "number of radiohalos per slide" column were obtained by summing all the radiohalos identified and counted for each rock unit, and then dividing the total by the number of slides examined for each rock unit to count those radiohalos. The figures in the "number of Po radiohalos per slide" were similarly obtained, except only the Po radiohalos counted were summed for each rock unit. Finally, the ratios of the numbers of the various radiohalos types to one another were calculated.

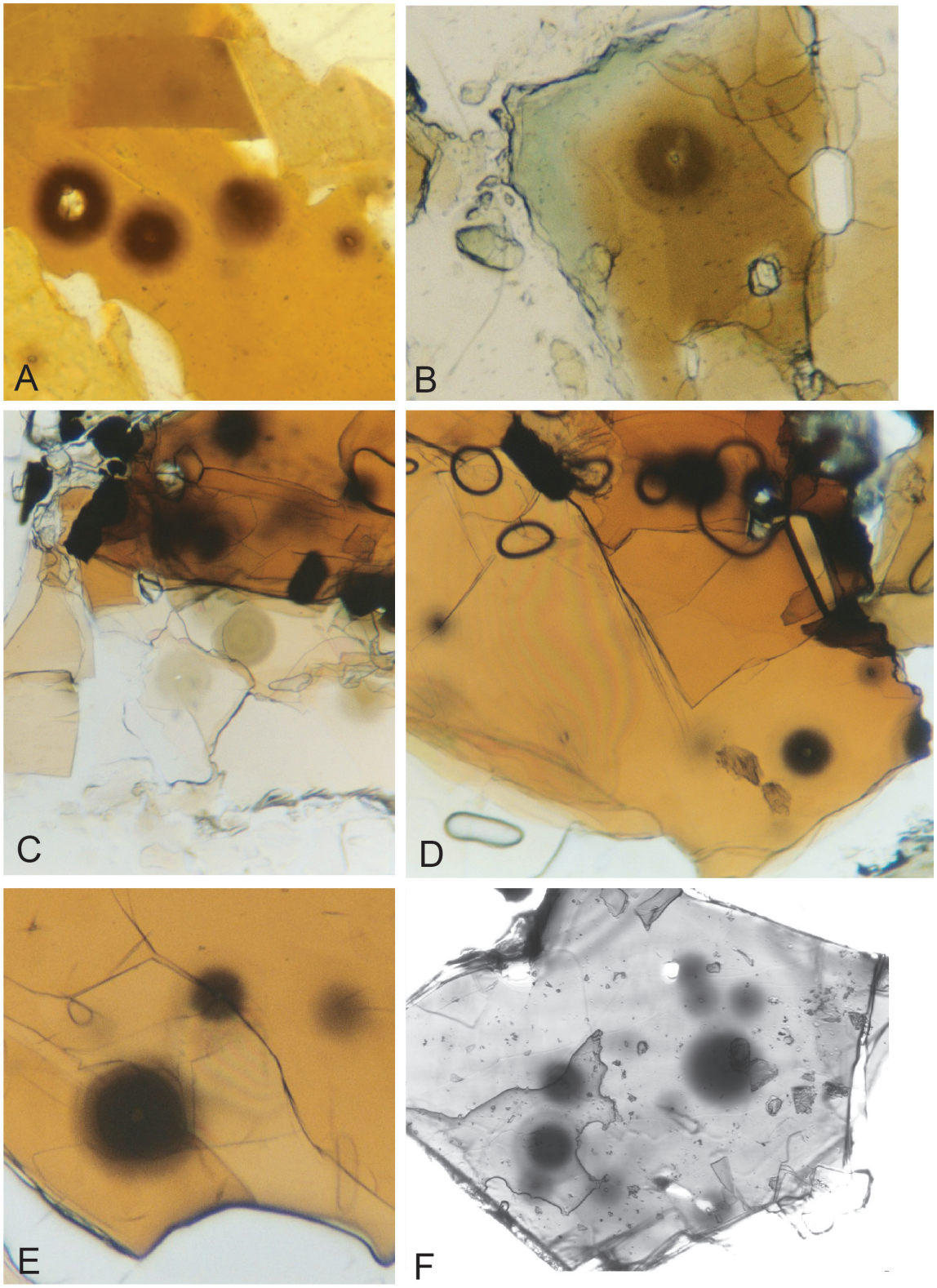

Figure 4. Some typical examples of the different radiohalos found in granites and metamorphic rocks. All images are in focus, but where the radiohalos appear fuzzy it is due to the intensity of the radiation broadening the outlines and the rings. The scales are provided with the following descriptions. (a) An overexposed ^{238}U radiohalo (Cooma Granodiorite, diameter ~70 µm, center) and a ^{210}Po radiohalo (diameter ~39 µm, right). (b) A well-exposed ^{238}U radiohalo (Shap Granite, diameter ~70 µm). (c) Two faint ^{218}Po radiohalos (Land's End Granite, diameter ~70 µm, center). (d) ^{238}U (diameter ~70 µm, upper center), ^{214}Po (diameter ~68 µm, lower right) and ^{210}Po (diameter ~39 µm, right) radiohalos together in the same biotite grain (Land's End Granite). (e) Another ^{214}Po radiohalo (centered on a crack) (Land's End Granite, diameter ~68 µm, right) and an overexposed ^{238}U radiohalo (diameter ~70 µm, left). (f) Overexposed ^{238}U radiohalos (Vishnu Schist, diameter ~70 µm) and ^{210}Po radiohalos (diameter ~39 µm).

Table 1. Radiohalos identified and counted in granitic rocks spanning the geologic record from the Archean to the present.

Rock Unit	Location	"Age"	Samples (slides)	Radiohalos					Number of Radiohalos per Slide	Number of Po Radiohalos per Slide	Ratios			
				^{210}Po	^{214}Po	^{218}Po	^{238}U	^{232}Th			^{210}Po:^{238}U	^{210}Po:^{214}Po	^{210}Po:^{218}Po	^{238}U:^{232}Th
Kingston Granite	Kingston Range, CA	Miocene	1 (50)	0	0	0	0	0	0	0	--	--	--	--
Granite	Phoenix, AZ	Early Miocene-Oligocene	2 (100)	0	0	0	0	0	0	0	--	--	--	--
Index Granite	Cascades, WA	Oligocene (33 Ma)	1 (50)	9	0	0	2	0	0.22	0.18	4.5:1	--	--	--
Spry Granite	Panguitch, UT	Oligocene	1 (50)	0	0	0	0	0	0	0	--	--	--	--
Granite	Salt Lake, UT	Tertiary	1 (50)	0	0	0	0	0	0	0	--	--	--	--
Chelan Granite	Pateros area, WA	Paleocene-Cretaceous	2 (100)	0	0	0	0	0	0	0	--	--	--	---
Granite	Phoenix, AZ	Late Cretaceous-early Tertiary	1 (50)	0	0	0	0	0	0	0	--	--	--	--
Bitterroot Batholith	Idaho, USA	70-90 Ma	4 (200)	38	0	0	18	0	0.28	0.19	2.1:1	--	--	--
Joseph Pluton, Idaho Batholith	Montana, USA	70-90 Ma	1 (50)	0	0	0	0	0	0	0	--	--	--	--
Butte Quartz Monzonite	Montana, USA	73-78 Ma	2 (100)	26	0	0	1	0	0.27	0.26	26:1	--	--	--
Mt Stuart Granite	Washington, USA	88 Ma	1 (50)	0	0	0	0	0	0	0	--	--	--	--
Black Peak Batholith	Washington, USA	Late Cretaceous	1 (50)	1	0	0	2	0	0.06	0.02	0.5:1	--	--	--
Golden Horn Granite			1 (50)	7	0	0	1	0	0.2	0.14	7:1	--	--	--
Seoul Granite	Seoul, South Korea	Late Cretaceous	1 (50)	300	0	0	171	0	9.42	6.0	1.75:1	--	--	--
Indian Hill Granite	San Diego County, USA	90 Ma	4 (180)	279	11	0	45	0	1.86	1.61	6.2:1	25.4:1	--	--
La Posta Pluton		93 Ma	8 (383)	96	4	0	8	0	0.3	0.26	8:1	24:1	--	--
Granodiorite of Mono Dome	Yosemite, USA	93 Ma	1 (50)	6	0	0	0	0	0.1	0.1	--	--	--	--
San Jacinto Pluton	Palm Springs, USA	Late Cretaceous	9 (450)	96	0	0	9	0	0.22	0.21	10.7:1	--	--	--
Johnson Granite Porphyry	Yosemite, USA	85-86 Ma	1 (50)	58	0	0	6	0	3.26	3.14	26:1	--	--	-
Cathedral Peak Granite	Yosemite, USA	87-88 Ma	2 (100)	325	0	0	6	0	3.31	3.25	54:1	--	--	--
Half Dome Granodiorite	Yosemite, USA	89-91 Ma	2 (100)	55	1	0	30	0	0.82	0.53	1.8:1	--	--	--
Granodiorite of Kuna Crest	Yosemite, USA	93-95 Ma	3 (150)	5	0	0	3	0	0.05	0.03	1.7:1	--	--	--
Yosemite Creek Granodiorite	Yosemite, USA	~93-95 Ma	2 (100)	8	0	0	0	0	0.08	0.08	--	--	--	--
Sentinel Granodiorite	Yosemite, USA	~93 Ma	3 (150)	29	0	0	29	0	0.39	0.19	1:1	--	--	--
Taft Granite	Yosemite, USA	~96 Ma	1 (50)	58	0	0	6	0	1.28	1.16	9.7:1	--	--	--
Granodiorite of Illilouette Creek	Yosemite, USA	~100 Ma	2 (100)	24	0	0	8	0	0.32	0.24	3:1	--	--	--
El Capitan Granite	Yosemite, USA	~102 Ma	4 (200)	179	0	0	17	0	0.98	0.90	10.5:1	--	--	--
Bass Lake Tonalite	Yosemite, USA	114 Ma	1 (50)	84	0	0	0	3	1.7	1.68	--	--	--	--
Ward Mountain Trondhjemite	Yosemite, USA	115 Ma	1 (50)	63	0	0	0	0	1.26	1.26	--	--	--	--
Granodiorite of Arch Rock	Yosemite, USA	114-117 Ma	2 (100)	106	0	7	10	0	1.23	1.13	10.6:1	--	15.1:1	--
Tonalite of the Gateway	Yosemite, USA	114-117 Ma	2 (100)	1	0	0	0	0	0.01	0.01	--	--	--	--
Conway Granite	New Hampshire, USA	175-188 Ma	9 (450)	1649	137	5	946	0	6.08	3.98	1.74:1	12:1	330:1	--

Table 1 continued

Wheeler Crest Granodiorite	Mammoth, USA	200-215 Ma	1 (50)	58	0	12	1	0	1.42	1.4	58:1	--	4.8:1	--
Lee Vining Canyon Granite	Yosemite, USA	200-215 Ma	1 (50)	108	0	20	13	0	2.46	2.2	8.3:1	--	54:1	--
Tent Hill Porphyrite	NSW, Australia	~230 Ma	1 (50)	0	0	0	0	0	0	0	--	--	--	--
Dundee Adamellite	NSW, Australia	~230 Ma	1 (50)	22	0	0	1	0	0.46	0.44	22:1	--	--	--
Sandy Flat Adamellite	NSW, Australia	~230-240 Ma	1 (50)	243	0	0	66	0	6.18	4.86	3.7:1	--	--	--
Stanthorpe Adamellite	Queensland, Australia	232 Ma	6 (298)	1395	5	15	168	19	5.38	4.75	8.3:1	279:1	93:1	8.8:1
Undercliffe Falls Granite	NSW, Australia	~240 Ma	1 (50)	3	0	0	0	0	0.06	0.06	--	--	--	--
Bolivia Range Adamellite	NSW, Australia	~240 Ma	1 (50)	235	0	0	59	0	5.88	4.70	4:1	--	--	--
Mole Granite	NSW, Australia	247.6 Ma	4 (200)	4474	0	0	2227	0	33.51	22.37	2.0:1	--	--	--
Uralla Granodiorite	NSW, Australia	~260 Ma	2 (100)	616	0	6	101	0	7.17	6.16	6.1:1	--	102.7:1	--
Mt Duval Adamellite	NSW, Australia	~260 Ma	1 (50)	335	0	0	167	0	10.04	6.70	2:1	--	--	--
Llangothlin Adamellite	NSW, Australia	~260 Ma	1 (50)	35	0	0	19	0	1.08	0.70	1.8:1	--	--	--
Shannonvale Granodiorite	NSW, Australia	~260 Ma	1 (50)	52	0	0	5	0	1.14	1.04	10.4:1	--	--	--
Royken/ Drammen Granite	Spikkestad, Norway	267±4 Ma	1 (100)	225	0	0	5	0	2.3	2.25	45:1	--	--	--
Finnamarka Granite	Gulsrudsetra, Norway	268±3 Ma	1 (50)	0	0	0	6	0	0.12	0	--	--	--	--
Thunderbolt Granite	Queensland, Australia	265-275 Ma	1 (50)	11	0	0	0	0	0.22	0.22	--	--	--	--
Land's End Granite	Cornwall, England	275 Ma	9 (432)	10,962	485	27	12,988	10	56.65	26.56	0.85:1	22.6:1	406:1.	1289:1
Cooktown Granite	Queensland, Australia	275 Ma	2 (100)	399	0	0	76	0	4.75	3.99	5.25:1	--	--	--
Tinaroo Granite	Queensland, Australia	270-280 Ma	1 (50)	787	0	0	1213	0	40	15.74	0.65:1	--	--	--
Moonbi Adamellite	NSW, Australia	~280 Ma	1 (50)	49	0	2	16	0	1.34	0.98	3.2:1	--	24.5:1	--
Kingsgate Granite	NSW, Australia	~280 Ma	1 (50)	113	0	0	26	0	2.78	2.26	4.4:1	--	--	--
Bungulla Adamellite	NSW, Australia	~280 Ma	1 (50)	156	0	0	27	0	3.66	3.12	5.5:1	--	--	--
Bellenden Ker Granite	Queensland, Australia	~280 Ma	1 (50)	818	0	0	422	0	24.8	16.36	1.94:1	--	--	--
Mareeba Granite	Queensland, Australia	275-285 Ma	1 (50)	285	0	0	111	0	7.92	5.7	2.57:1	--	--	--
Tully Granite	Queensland, Australia	286 Ma	1 (50)	163	0	0	15	0	3.56	3.26	10.9:1	--	--	--
Bodmin Moor Granite	Cornwall, England	290 Ma	2 (100)	993	0	0	2714	0	37.07	9.93	0.37:1	--	--	--
Stone Mountain Pluton	Georgia, USA	291±7 Ma	6 (291)	1109	93	2	88	0	4.44	4.14	12.6:1	12:1	554.5:1	--
Petersburg Granite	Virginia, USA	260-325 Ma	1 (50)	4	0	0	0	0	0.08	0.08	--	--	--	--
Liberty Hill Pluton	Lancaster, SC	299±48 Ma	3 (150)	180	0	0	0	0	1.2	1.2	--	--	--	--
Almaden Granite	Queensland, Australia	290-308 Ma	1 (50)	1562	0	0	364	0	38.52	31.24	4.29:1	--	--	--
Bendemeer Adamellite	NSW, Australia	~300 Ma	1 (50)	83	0	0	52	0	2.70	1.66	1.6:1	--	--	--
Hillgrove Granite	NSW, Australia	~300 Ma	3 (150)	853	8	0	1094	0	12.83	5.74	0.78:1	106.6:1	--	--
Hammonds Creek Granodiorite	Queensland, Australia	300-305 Ma	2 (100)	679	0	0	83	0	7.62	6.79	8.18:1	--	--	--

Table 1 continued

Bathurst Granite	NSW, Australia	330 Ma	12 (602)	3438	24	527	1993	31	9.99	6.63	1.73:1	143.3:1	6.52:1	64.3:1
Carcoar Granite	NSW, Australia	~330 Ma	2 (100)	38	0	0	7	0	0.45	0.38	5.43:1	--	--	--
Evans Crown Dike	NSW, Australia	330 Ma	8 (400)	227	0	0	34	0	0.65	0.57	6.68:1	--	--	--
Spruce Pine pegmatites	North Carolina, USA	~340 Ma	3 (150)	1451	71	182	66	0	11.8	11.36	22:1	20.4:1	8:1	--
Mt Airy Granite	North Carolina, USA	~350 Ma	2(100)	1271	22	0	120	0	14.13	12.93	10.6:1	57.8:1	--	--
Stone Mountain Granite	North Carolina, USA	~350 Ma	2(100)	1543	4	174	5	0	17.26	17.21	309:1	386:1	8.9:1	--
Bicheno Adamellite	Tasmania, Australia	355-380 Ma	3 (150)	1668	0	7	376	0	13.67	11.17	4.44:1	--	238:1	--
Heemskirk Granite	Tasmania, Australia	360-365 Ma	1 (50)	307	1	0	19	0	0.4	0.05	0.05:1	--	--	--
Coles Bay Granite	Tasmania, Australia	360-370 Ma	3 (150)	630	1	3	122	0	5.01	4.2	5.16:1	--	--	--
Harcourt Granite	Victoria, Australia	369 Ma	1 (31)	107	130	0	198	0	14.03	7.65	0.54:1	0.82:1	--	--
Strathbogie Granite	Victoria, Australia	374 Ma	1 (50)	1366	232	1	1582	10	63.82	31.98	0.86:1	5.9:1	1366:1	158.2:1
Willoughby Granite	NE Vermont, USA	376 Ma	3 (50)	1926	0	0	899	0	18.83	12.84	2.14:1	--	--	--
Bowen Granite	Queensland, Australia	378-386 Ma	3 (150)	45	0	0	1	0	0.31	0.3	45:1	--	--	--
Dumbano Granite	Queensland, Australia	378-399 Ma	1 (50)	18	0	0	0	0	0.36	0.36	--	--	--	--
Shap Granite	Lake District, England	393 Ma	4 (204)	1912	19	16	618	40	12.82	9.54	3.1:1	100.6:1	119.5:1	12.4:1
Shannons Flat Granite	NSW, Australia	417-443 Ma	1 (101)	9	18	0	38	0	0.64	0.27	1:4.2	1:2	--	--
Jillamatong Granite	NSW, Australia	417-443 Ma	1 (31)	120	118	0	137	0	12.1	7.68	1:1.1	1:1	--	--
Cootralantra Granite	NSW, Australia	417-443 Ma	1 (43)	230	75	0	276	2	13.56	7.1	1:1.2	3.1:1	--	138:1
Cooma Granodiorite	NSW, Australia	433 Ma	2 (91)	1548	44	81	736	37	26.88	18.38	2:1.1	35.1:1	19.1:1	19.9:1
Encounter Bay Granite	South Australia	487-490 Ma	1 (45)	362	8	0	1586	161	47.04	8.22	1:4.4	45.3:1	--	9.9:1
Palmer Granite	South Australia	490 Ma	1 (51)	1352	17	0	631	3	39.3	26.84	2.1:1	79.5:1	--	210.3:1
Timna Monzodiorite	Timna, Israel	599 Ma	3 (150)	134	0	0	6	0	0.93	0.89	22.3:1	--	--	--
Granite (Methrow)	Washington, USA)	600 Ma?	1 (50)	1	0	0	0	0	0.02	0.02	--	--	--	--
Timna alkali granite	Timna, Israel	609 Ma	2 (100)	0	0	0	0	0	0	0	--	--	--	--
Cape Granite	Cape Town, South Africa	630 Ma	3 (150)	220	0	0	488	0	4.72	1.47	0.45:1	--	--	--

Table 1 continued

Roded porphyritic granite	Shehoret Canyon, Israel	634 Ma	5 (250)	63	0	0	3	0	0.26	0.25	21:1	--	--	--
Lovingston Granite Gneiss	Virginia, USA	Meso-Proterozoic (1022-1043 Ma ?)	3 (150)	40	0	0	0	0	0.27	0.27	--	--	--	--
Pikes Peak Granite	Colorado, USA	1080 Ma	1 (51)	80	2	0	8	0	1.8	1.6	10:1	40:1	--	--
Lake George Granite		1080 Ma	1 (51)	12	0	0	14	0	0.5	0.24	1:1.2	--	--	--
Sherman Granite	Wyoming, USA	1400 Ma	1 (50)	4	0	0	0	0	0.1	0.1	--	--	--	--
Ruin Granite	Arizona, USA	1430 Ma	1 (41)	176	1	0	10	0	4.6	4.3	17.6:1	176:1	--	--
Baltimore Gneiss	Maryland, USA	Meso-Proterozoic	2 (100)	128	0	0	31	0	1.59	1.28	4.13:1	--	--	--
Jemez Granodiorite	New Mexico, USA	1500 Ma	1 (33)	29	1	0	14	0	1.3	0.91	2.1:1	29:1	--	--
Granite (Unaweep Canyon)	Colorado, USA	1500 Ma (?)	1 (50)	19	0	1	0	0	0.4	0.4	--	--	19:1	--
Orbicular Granite (Shoup)	Idaho, USA	1500 Ma	1 (50)	9	0	1	4	0	0.3	0.2	2.3:1	--	9:1	--
Bright Angel Granite	Grand Canyon, USA	1662 Ma (?)	3 (150)	278	0	0	269	0	3.65	1.85	1.03:1	--	--	--
Cottonwood Pegmatite	Grand Canyon, USA	1680-1685 Ma	2 (100)	0	0	0	1	0	0.01	0.01	--	--	--	--
Sapphire Pegmatite	Grand Canyon, USA	(?) 1690 Ma	3 (150)	3	0	0	0	0	0.02	0.02	--	--	--	-
Pipe Creek Granite	Grand Canyon, USA	1690-1740 Ma (?)	1 (50)	132	0	0	0	0	2.64	2.64	--	--	--	--
Horn Creek Granite	Grand Canyon, USA	1713 Ma	8 (400)	1047	0	0	193	0	3.1	2.62	5.4:1	--	--	--
Ruby Granodiorite	Grand Canyon, USA	1716 Ma	12 (600)	3206	0	0	1449	0	7.75	5.34	2.2:1	--	--	--
Granite Narrows Granite	Grand Canyon, USA	1716-1736 Ma (?)	5 (250)	177	0	0	32	0	0.34	0.71	5.53:1	--	--	--
Trinity Granodiorite	Grand Canyon, USA	1730 Ma	10 (500)	713	2	0	355	0	2.14	1.43	2:1	365.5:1	--	--
Diamond Creek Granite	Grand Canyon, USA	1736 Ma	4 (200)	11	0	0	0	0	0.22	0.22	--	--	--	--
Zoroaster Granite	Grand Canyon, USA	1740 Ma	5 (250)	1245	0	0	228	0	5.89	4.98	5.46:1	--	--	--
Helsinki Granite	Helsinki, Finland	1800 Ma	3 (150)	107	1	0	241	0	2.3	0.72	0.44:1	107:1	--	--
Elves Chasm Granodiorite	Grand Canyon, USA	1840 Ma	13 (650)	93	0	0	27	0	0.18	0.14	3.44:1	--	--	--
Owl Creek Granite	Wyoming, USA	2500 Ma	1 (50)	5	0	0	0	0	0.1	0.1	--	--	--	--
Nanambu Granite	Pine Creek Basin, Australia	2560 Ma (?)	3 (150)	212	0	0	184	0	2.64	1.41	1.15:1	--	--	--
Namban Granite	Yilgarn, Western Australia	2670-2689 Ma	1 (41)	318	16	0	120	3	10.7	8.15	2.7:1	19.9:1	--	40:1
Badja Granite			1 (43)	188	0	0	58	0	5.7	4.37	3.2:1	--	--	--
Rattlesnake Granite	Wyoming, USA	2800-2900 Ma	1 (50)	10	0	0	25	0	0.7	0.2	1:2.5	--	--	--
Bighorn Granite			1 (50)	0	0	0	0	0	0	0	--	--	--	--
Granite Gneiss	Minnesota, USA	Late Archean	1 (50)	29	0	0	9	0	0.76	0.58	3.22:1	--	--	--
Granite Gneiss	Minnesota, USA	Late Archean	1 (50)	14	0	0	6	0	0.4	0.28	2.33:1	--	--	--
Granite Gneiss	Minnesota, USA	Late Archean	1 (50)	3	0	0	2	0	0.1	0.06	1.5:1	--	--	--

Table 1 continued

Granite Gneiss	Minnesota, USA	Late Archean	1 (50)	6	0	0	5	0	0.22	0.12	1.2:1	--	--	--
Granite (tonalites)	Ilomantsi, Finland	Archean	3 (150)	85	0	0	0	0	0.6	0.6	--	--	--	--
Granite Gneiss	Minnesota, USA	Middle to Lower Archean	1 (50)	48	0	0	28	0	1.52	0.96	1.71:1	--	--	--

Table 2. Radiohalos identified and counted in regional metamorphic rocks spanning the geologic record from the Archean to the lower Phanerozoic.

Rock Unit	Location	"Age"	Samples (slides)	Radiohalos					Number of Radiohalos per slide	Number ofPo Radiohalos per slide	Ratios			
				^{210}Po	^{214}Po	^{218}Po	^{238}U	^{232}Th			^{210}Po:^{238}U	^{210}Po:^{214}Po	^{210}Po:^{218}Po	^{238}U:^{232}Th
Cooma Metamorphic Complex	NSW, Australia	410-433 Ma	7 (350)	3368	76	1	727	0	11.92	9.84	4.63:1	44.3:1	3368:1	--
Migmatite adjacent to Palmer Granite	South Australia	Ordovician	1(51)	234	8	0	507	3	14.75	4.75	1:2.2	29.3:1	--	169:1
Biotite Garnet Eclogite	Stordal, Norway	Upper Proterozoic	1 (50)	7	0	0	0	0	0.14	0.14	--	--	--	--
Thunderhead Sandstone	Tennessee-North Carolina (USA)	Upper Proterozoic	10 (500)	522	19	0	0	0	1.08	1.08	--	24.5:1	--	--
Metamorphic pegmatite	Steiggjelselva, Norway	Middle to Upper Proterozoic	1 (50)	30	0	0	0	0	0.6	0.6	--	--	--	--
Gneiss (and pegmatite)	Hegland, Norway	Lower Proterozoic	2 (100)	0	0	0	0	0	0	0	--	--	--	--
Gneiss (and pegmatite)	Arendal, Norway	Proterozoic	2 (100)	65	33	0	0	0	0.98	0.98	--	1.97:1	--	--
Gneiss	Sandbraten, Norway	Proterozoic	1 (50)	78	0	0	0	0	1.56	1.56	--	--	--	--
Gneiss	Gravfoss, Norway	Proterozoic	1 (50)	0	0	0	0	0	0	0	--	--	--	--
Sundown Group	Broken Hill, NSW, Australia	1670-1680 Ma	1 (50)	20	0	0	0	0	0.4	0.4	--	--	--	--
Rasp Ridge Gneiss	Broken Hill, NSW, Australia	1683 Ma	6 (300)	1626	0	0	788	0	8.04	5.42	2.06:1	--	--	--
Hores Gneiss	Broken Hill, NSW, Australia	1685 Ma	17 (850)	5374	3	2	2459	0	9.22	6.32	2.19:1	1791:1	2687:1	--
Amphibolites in Hores Gneiss	Broken Hill, NSW, Australia	1685 Ma	3 (150)	10	0	0	0	0	0.67	0.67	--	--	--	--
Purnamoota Sub-Group (undifferent.)	Broken Hill, NSW, Australia	1685-1693 Ma	2 (100)	365	0	0	99	0	4.64	3.65	3.69:1	--	--	--
Amphibolites in Parnell Formation	Broken Hill, NSW, Australia	1692-1693 Ma	3 (150)	43	0	0	0	0	0.29	0.29	--	--	--	--
Allendale Meta-sediments	Broken Hill, NSW, Australia	1693 Ma	1 (50)	7	0	0	0	0	0.14	0.14	--	--	--	--
Thackaringa Group	Broken Hill, NSW, Australia	~1700 Ma	2 (100)	445	1	0	0	0	4.46	4.46	--	445:1	--	--
Vishnu Schist	Grand Canyon, USA	1730-1750 Ma	30 (1500)	18,523	14	4	11,308	0	19.9	12.36	1.64:1	1323:1	4631:1	--
Rama Schist	Grand Canyon, USA	1730-1750 Ma	13 (650)	2398	0	0	1292	0	5.68	3.69	1.86:1	--	--	--
Beartooth Gneiss	Montana, USA	2790 Ma	5 (250)	1254	0	0	259	0	6.05	5.02	4.84:1	--	--	--
Biotite Schist	Minnesota, USA	Late Archean	1 (50)	14	0	0	3	0	0.34	0.28	4.67:1	--	--	--

Table 2 continued

Dyrkorn Gneiss	Sunnmøre, Norway	Archean	1 (50)	24	0	7	5	0	0.72	0.62	4.8:1	--	3.4:1	--
Gneiss	Ilomantsi, Finland	Archean	1 (50)	83	0	0	29	0	2.24	1.66	2.9:1	--	--	--

These tabulated radiohalos data were then plotted by hand on a graph with the conventional ages of the rock units in millions of years from 0-3500 Ma (x-axis) versus the number of radiohalos per slide (y-axis) in each rock unit (Fig. 5). Granites were distinguished from metamorphic rocks by different symbols. It should immediately be evident from Table 1 and Fig. 5 that many samples cluster within the shorter conventional time range of the Phanerozoic (0-539 Ma) compared with the wider spread of the Precambrian (>539 Ma) samples. Thus, for ease of identifying any trends in the radiohalos data for the Phanerozoic rock units, those data were hand plotted on a similar graph with only a conventional age spread of 0-600 Ma on the enlarged x-axis (Fig. 6).

V. DISCUSSION

It is assumed for the purposes of this study that the conventional ages are valid within the conventional paradigm, but they are used here only to identify the relative positions of the rock units in the geologic record. While it has been well-demonstrated that there are numerous significant problems with each of the long-age radioactive dating methods that preclude the obtained ages from being absolute ages (Snelling 2000a), there is still a systematic trend in conventionally-published radioactive ages of rocks according to those rocks' relative positions in the geologic record. In other words, the oldest-aged rocks are found at the observationally-established bases of local rock sequences, and the observationally-established overlying and intruded rocks units decrease in age according to the relative order of formation of the rock units (Snelling 2005b, c, Vardiman et al. 2005).

If it is established that there was a pulse of five-orders-of-magnitude accelerated radioactive decay with accompanying heat during the Flood (Vardiman et al. 2005), then all pre-Flood and Creation Week rocks would have been affected by that pulse of accelerated radioactive decay with accompanying heat. And since it has been demonstrated observationally that radiohalos are annealed (wiped out) above a temperature of only 150°C (Laney and Laughlin 1981), then any radiohalos in them produced before the Flood would have been annealed by that pulse of accelerated radioactive decay with accompanying heat. Thus, the radiohalos we observe today in pre-Flood and Creation Week rocks would have been produced in them during the Flood after they had again cooled below150°C. This needs to be kept in mind when interpreting the radiohalos data tabulated in this study (Tables 1 and 2).

From the radiohalos frequency data plotted in Fig. 5 it should be immediately evident that:

(1) There is clear difference between the radiohalos frequencies in Phanerozoic (0-539 Ma) granites compared to Precambrian (>539 Ma) granites. Indeed, radiohalos frequencies rise dramatically from the average range of about 0-15 radiohalos per slide in most Phanerozoic and all Precambrian granites to a range of 25-64 radiohalos per slide in some Phanerozoic granites, for example, the Mole Granite, Land's End Granite, Tinaroo Granite, Bodmin Moor Granite, Alamaden Granite, Strathbogie Granite, Encounter Bay Granite, and the Palmer Granite (Table 1). In contrast, the Precambrian granites have a range of only 0-10 radiohalos per slide.

(2) The radiohalos frequency in Phanerozoic and Precambrian regional metamorphics rocks are generally the same range at 0-15 radiohalos per slide, similar to the range of radiohalos frequency in most Phanerozoic and all Precambrian granites. However, whereas the average range of radiohalos frequency in most regional metamorphic rocks is 0-5 radiohalos per slide, there are some regional metamorphic rocks that stand out with a range of 10-15 radiohalos per slide, for example, the Precambrian Vishnu Schist and the Phanerozoic Cooma Metamorphic complex, and the migmatite associated with the Palmer Granite (Table 2).

(3) There are lots of "time" gaps in the spread of Precambrian samples, both granites and the regional metamorphic rocks clumping together. In fact, there appears to be some clear groupings, namely, peaks at about 1400-1850 Ma and about 2550-3200 Ma, plus another tiny peak around 600-700 Ma among the Precambrian samples, and then from 0-500 Ma in the Phanerozoic as a whole.

Where the timescale for the Phanerozoic has been expanded in Fig. 6, similar observations are evident:

(1) The radiohalos frequencies are well above the average 0-15 radiohalos per slide for the granites generally in the Mole Granite (c.33), Land's End Granite (c.57), Tinaroo Granite (40), Bodmin Moor Granite (c.37), Alamaden Granite (c.38), Strathbogie Granite (c.64), Encounter Bay Granite (c.47), and the Palmer Granite (c.39).

(2) The paucity of samples of Phanerozoic regional metamorphic rocks does not permit comparisons between such rock units, the Cooma Metamorphic complex (c.12) and the migmatite associated with the Palmer Granite (c.15) do still stand out at the high end of the 0-15 radiohalos per slide average range as found in most of the Phanerozoic granites.

(3) There is also a possible peaking of the Phanerozoic radiohalos frequency data from about 200 Ma to 500 Ma. That corresponds to the Triassic to upper middle Cambrian or primarily the Paleozoic. Furthermore, after a tiny secondary peak in the radiohalos frequency data between about 70 Ma and 130 Ma (essentially the Cretaceous) there are hardly any radiohalos in subsequent granites (Paleogene and Neogene).

Of course, it must be recognized that some of these observations could be biased by the spread of sampling. There are some obvious apparent sampling gaps in Figs. 5 and 6 where there are no granites or regional metamorphic rocks plotted. However, these gaps might also represent a lack of granites or regional metamorphic rocks of those apparent ages in the rock record, for example, between 2000 Ma and 2500 Ma, between 500 Ma and 600 Ma, and between 130

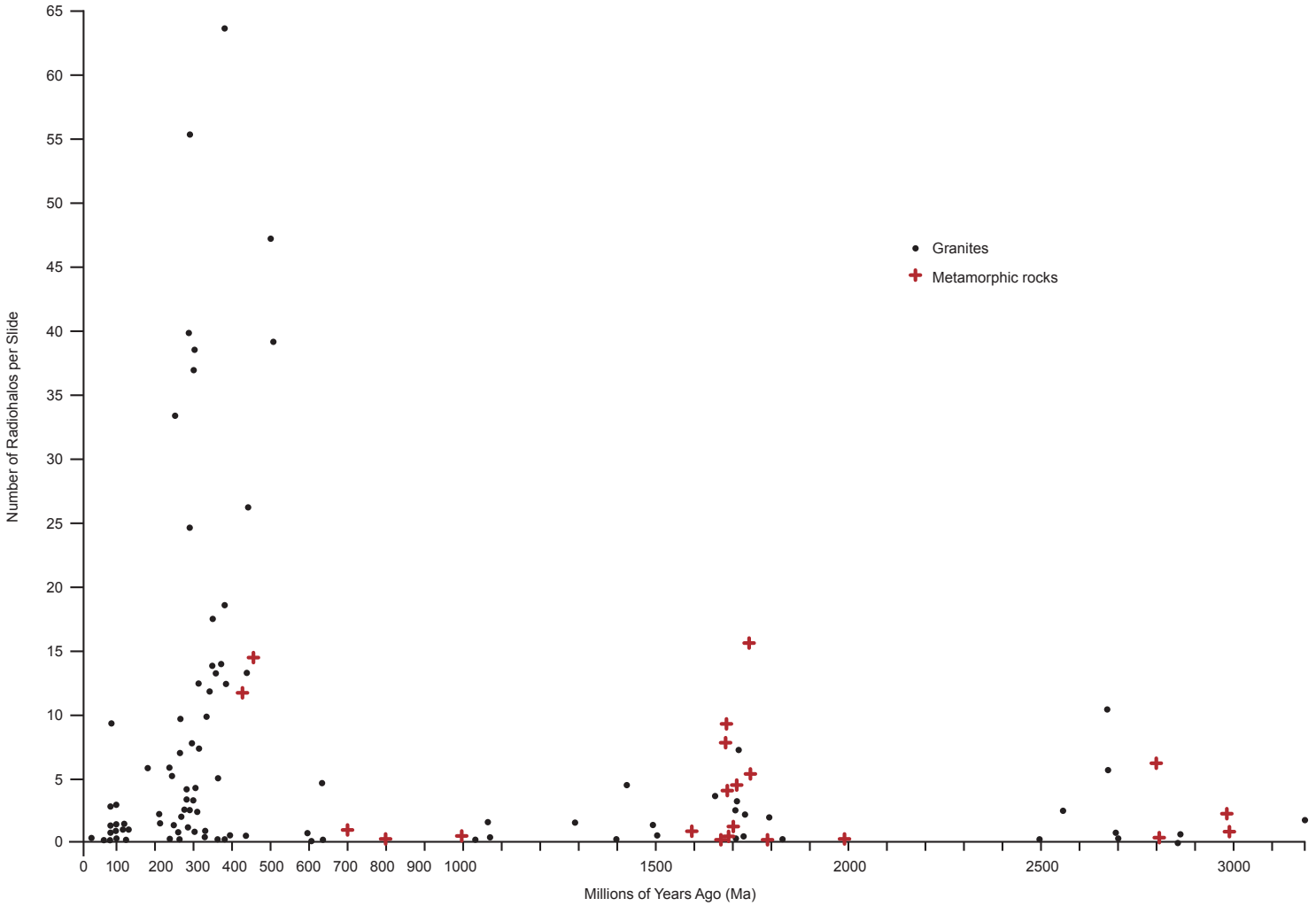

Figure 5. Plot of the number of radiohalos per slide (y-axis) for each rock unit in Tables 1 and 2 versus the conventional age in millions of years (x-axis) from 0-3500 Ma. The granites are marked with dots and the metamorphic rock units with red crosses.

Ma and 180 Ma. Nevertheless, these observations raise several clear issues that require discussion.

A. The pre-Flood/Flood boundary

Austin and Wise (1994) and Whitmore and Garner (2008) established some definitive guidelines for recognizing the pre-Flood/Flood boundary in the geologic record. They then applied those guidelines in two areas, the Mohave–Grand Canyon region and Wyoming, respectively, to conclude that the pre-Flood/Flood boundary approximated to the Cambrian/Precambrian in the rock record. This corresponds in North America to the Great Unconformity, which has been recognized as essentially a global, massive erosional event horizon (Peters and Gaines 2012) that would thus correlate with the onset of the Flood.

The radiohalos frequency data tabulated in this study and plotted in Fig. 5 appear to be consistent with Cambrian/Precambrian boundary in the rock record being approximately the pre-Flood/Flood boundary. Admittedly, this determination based on radiohalos frequency is not definitive, as there is an already-noted paucity of data between 500 Ma and 600 Ma. Furthermore, if that gap in data were filled it might thus incorporate the tiny 600-700 Ma peak into the 200-500 Ma peak, and then it might be argued that the pre-Flood/Flood boundary could be earlier in the geologic record than the Cambrian/Precambrian boundary.

However, it is the 200-500 Ma peak dominated by numerous granites with extraordinarily high radiohalos frequency per slide which would clearly correlate with the Flood. Namely, granites that formed during the Flood expelled water as they crystallized and cooled that facilitated the generation of many radiohalos. In contrast, if the Precambrian granites are pre-Flood, then when the Flood came they were already crystallized and cooled. Thus, during the Flood they were only heated again by the pulse of accelerated radioactive decay of whatever ^{238}U was still in them, and there was not the same amount of water available in those already-crystallized granites to generate many radiohalos to replace those annealed by the pulse of accompanying heat.

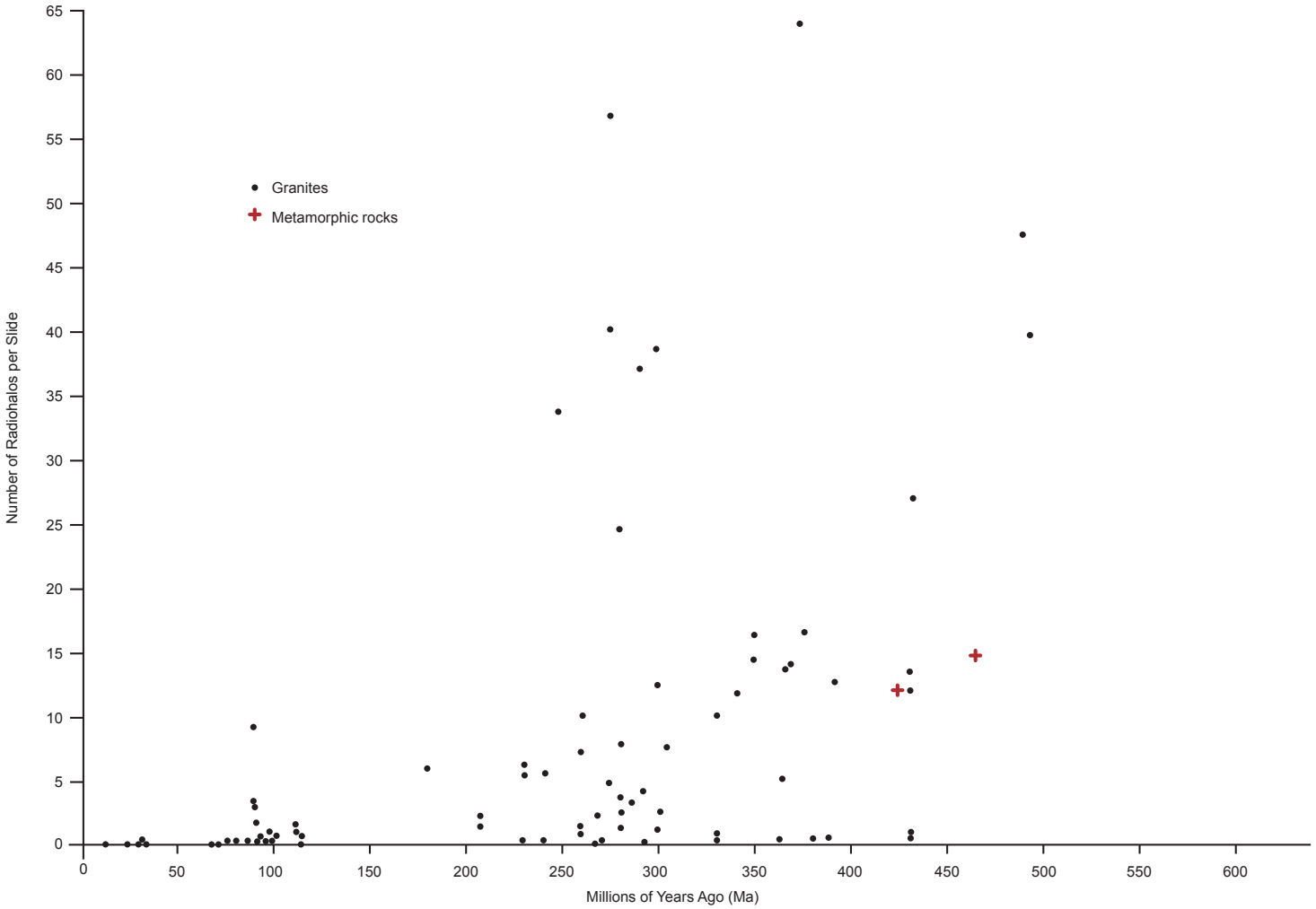

Figure 6. Plot of the number of radiohalos per slide for each rock unit in Tables 1 and 2 (y-axis) versus the conventional age in millions of years from 0-600 Ma (enlarged x-axis). The granites are marked with dots and the metamorphic rock units with red crosses.

B. The periodicity of granites and regional metamorphic rocks in the geologic record

What do we then make of the dominant peaks in the Precambrian rock record at about 1400-1850 Ma and about 2550-3200 Ma? Are those peaks due to sampling bias, or is there another explanation?

Condie et al. (2009) and Voice et al. (2011) have demonstrated that there are periodic peaks in the formation ages of granites in the Precambrian rock record. They based this on the U-Pb ages of detrital zircons that corresponded to the formation ages of the granites from which they were eroded. Fig. 7 is a plot of the frequency of 100,445 ≤ 5% discordant-filtered pooled U-Pb dated detrital zircon grains versus geologic age (after Voice et al 2011). It can be clearly seen that there are pronounced peaks at about 900-1350 Ma, at about 1650-2000 Ma, and at about 2350-2900 Ma.

Nance et al. (2014) correlated these peaks with the conventionally-proposed supercontinent cycle. Within the conventional paradigm this correlation is valid because the formation of granites and regional metamorphic rocks is controlled by the global tectonics that produced the supercontinent cycle, these rocks forming in mountain-building collision zones and adjacent to subduction zones, and also in island arcs.

While it is evident that the radiohalos frequency peaks in the Precambrian record in Fig. 5 do not exactly match those in Fig. 7, there is still a one-to-one reasonable correlation, given the sparse sampling of Precambrian granites and regional metamorphic rocks in this study. Indeed, the data reproduced in Fig. 7 represent over 100,445 U-Pb ages of detrital zircons (although eroded from an unidentified lesser number of granites and regional metamorphic rocks), whereas this study is based on some 147 granites and regional metamorphic rocks (although some data were gathered from multiple samples per rock unit). It is to be expected that further sampling of infill-aged rock units for radiohalos study would merely flesh-out the same peaks as in Fig.7. At least the comparison is also reasonable, given that it is tiny zircon inclusions in biotite grains in the granites and regional metamorphic rocks that produced the radiohalos due to the α-decay of their contained ^{238}U.

So, if these radiohalos frequency and detrital zircon U-Pb ages peaks are real, essentially coincide, and represent actual tectonic activity

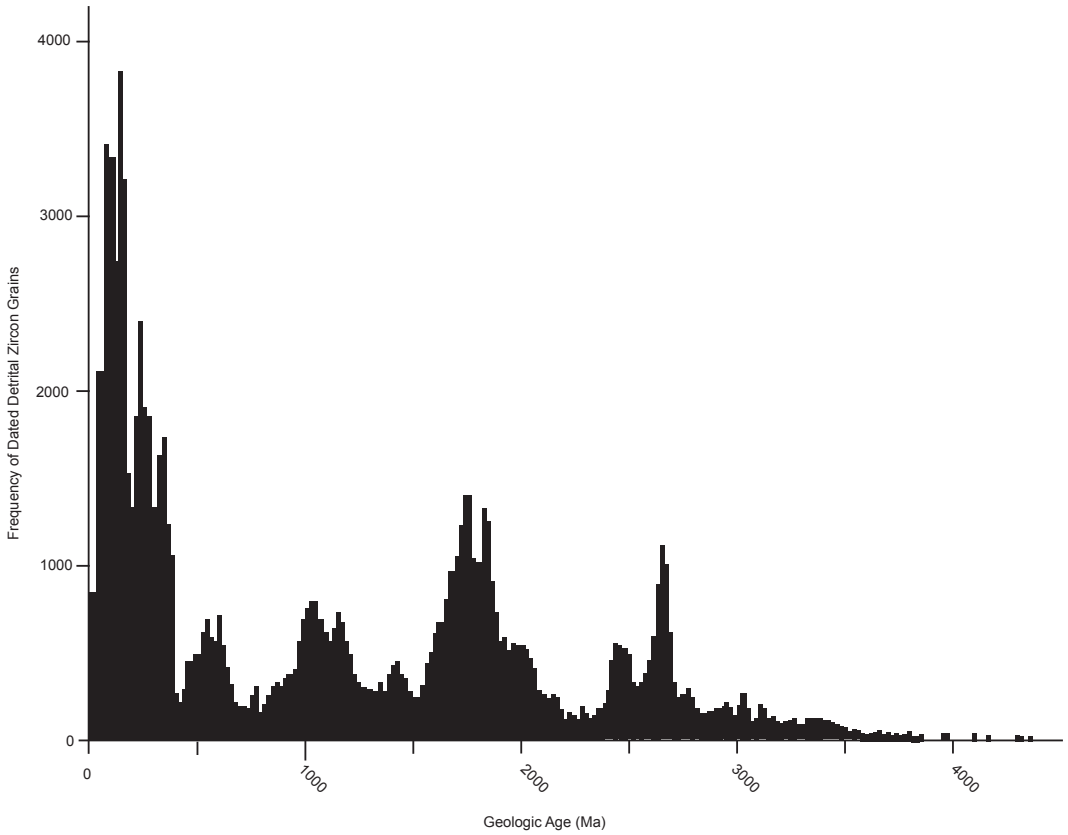

Figure 7. Plot of the frequency of 100,445 ≤ 5% discordant-filtered pooled U-Pb dated detrital zircon grains versus geologic age (after Voice et al. 2011).

that resulted in the formation of granites and regional metamorphic rocks, then how may this be interpreted with the Biblical framework of earth history?

Dickens and Snelling (2008) and Dickens (2018) have suggested that these peaks may represent the results of God's creative work in the first three days of the Creation Week. Of course, they are not diminishing the unique, miraculous, essentially instant creation by God when Genesis 1 says God spoke and it was so. The timescale was totally collapsed, so that what conventional geologists have claimed took billions of years, God accomplished instantly, but in the orderly sequence as also described in Genesis 1. Thus, each of these peaks (from "oldest" to "youngest") might represent the initial created rocks on Day 1, the effects on the initially-created rocks of God separating the waters to create the expanse between them on Day 2, and then the uplifting of some of the initial foundation rocks to form the dry land on Day 3, which would have resulted in erosion of those uplifted foundation rocks as they breeched the waters' surface and thus the deposition of sedimentary layers adjacent to the dry land and overlaying that erosion surface (Snelling 2009, 2022).

What then is the significance of the biggest peak at about 0-450 Ma in the Voice et al. (2011) data plotted in Fig. 7, with a secondary small peak at about 450-750 Ma. These peaks coincide with the latest global plate tectonics episodes of the supercontinent cycle. First was the breakup of Rodinia to form Gondwana and then eventually Pangaea (Nance et al. 2014). The 0-450 Ma peak is the biggest because it represents the latest cycle of erosion of the latest-formed granites and regional metamorphic rocks. The later-formed granites and regional metamorphic rocks are better preserved than earlier-formed granites and regional metamorphic rocks which have been deeply eroded and in some instances eroded away almost entirely, or they have been buried deeply underneath the latest sedimentary rocks of the Phanerozoic.

The radiohaloes frequency data plotted in Figs. 5 and 6 essentially represent the frequency of radiohalos production during the Flood due to the heat of Flood tectonic activity having annealed any previously-formed radiohalos. Thus, it is not surprising that the highest peak in radiohalos frequency would be in the granites produced during the Flood. Figs. 5 and 6 show radiohalos generation peaking at 200-500 Ma, which would potentially represent the tectonic activity in about the first half of the Flood. This is consistent with catastrophic plate tectonics as the driving mechanism of the year-long Flood, as proposed by Austin et al. (1994) and Baumgardner (2003), in contrast to the conventional timescale of 500-750 million years.

However, as already noted, this 200-500 Ma peak in the radiohalos frequency data does not fully match the shape of the 0-450 Ma peak in the Voice et al. (2011) data plotted in Fig. 7. Specifically, in Fig. 7 the highest portion of that peak is approximately in the 0-200 Ma range, reflecting the last part of the supercontinent cycle in which today's ocean basins opened and today's mountains formed in the plate collision zones and adjacent subduction zones. While some of this lack of matching of the radiohalos frequency data in the 0-450 Ma interval in Figs. 5 and 6 with the detrital zircon U-Pb ages in Fig. 7 is likely due to not enough sampling of granites in the 0-200 Ma range in this study, there is also another viable explanation. After all,

there is a small peak in the radiohalos frequency data in Fig. 6 around 80-120 Ma, but that is dominated by one granite.

However, more sampling of Phanerozoic granites, including those claimed to be 0-200 Ma in age, would potentially provide infill data in Fig. 6. Nevertheless, the most recent granites might not have many radiohalos in them anyway, as evident in Table 1 and Fig. 6, due to 100 million years' worth of accelerated ^{238}U (at today's measured rate) being needed to form good visible radiohalos. Also, the grossly accelerated ^{238}U decay rate during the Flood may have started to rapidly decelerate as the Flood ended and tectonic activity also started to decelerate.

C. Hydrothermal fluid activity during the Flood

In most instances, the granites and regional metamorphic rocks listed in Tables 1 and 2 have Po radiohalos in them, often more in number than the ^{238}U radiohalos they accompany frequently in the same biotite grains (91 out of 124 granites or ~73%, and 20 out of 23 metamorphic rocks or ~87%) (Fig 4). According to the hydrothermal fluid transport model for the formation of Po radiohalos (Snelling and Armitage 2003; Snelling 2005a) the greater the number of Po radiohalos in a granite or regional metamorphic rock is due to greater water flow, that is, hydrothermal fluid activity. This was predicted and then verified in case studies by Snelling (2008b, c, d, 2014, 2018) and Snelling and Gates (2009). Furthermore, many of the granites with the highest radiohalos frequency (Tables 1 and 2, Figs. 5 and 6) are granites that host or are genetically associated with hydrothermal metallic ore deposits, such as the Land's End and Bodmin Moor Granites of England (Moscati and Neymark 2020), and the Hillgrove and Mole Granites of the New England region of eastern Australia (Ashley et al. 1994: Ashley and Craw 2004; Audétat et al. 2000a, b; Comsti and Taylor 1984; Kleeman et al. 1997; Schaltegger et al. 2000). Indeed, Snelling (2018) demonstrated that the Po radiohalos in the latter two granites correlated with the hydrothermal ore veins and could thus be used as an exploration pathfinder for other hydrothermal ore deposits associated with unexplored granites.

The hydrothermal fluid activity during the Flood is thus easily recognized in Figs. 5 and 6, as just discussed. However, what of the smaller peaks in radiohalos frequency in the Precambrian (or pre-Flood) granites and regional metamorphic rocks in Fig. 5? Since any previously-generated radiohalos in these rocks would have been annealed as these rocks were subjected to the heat generated by the accelerated decay of any ^{238}U still in them during the Flood, the Po radiohalos now observed in these rocks must be due to hydrothermal activity during the Flood.

Yet, according to the hydrothermal fluid transport model for Po radiohalos formation (Snelling and Armitage 2003; Snelling 2005a, Snelling 2008a), the peak window for hydrothermal fluid activity and thus the formation of Po radiohalos is after the heat involved in the formation of the host rocks is waning and those host rocks have cooled below 150°C. However, by the time of the onset of the Flood those Precambrian granites and regional metamorphic rocks had already formed and cooled. Thus, the Po radiohalos now observed in them had to be generated by the heating during the Flood of whatever ground water had penetrated into them in the pre-Flood world, and/or by whatever hydrothermal fluids were injected into them during the Flood. By either process those pre-Flood rocks would have been less proficient at generating copious quantities of Po radiohalos, certainly not at the levels of "freshly-made" Flood granites, especially those that expelled huge amounts of hydrothermal fluids from the granitic magmatic fluids to also produce associated metallic ore veins.

So why would the Precambrian regional metamorphic rocks in many instances be better at generating new Po radiohalos during the Flood compared to the Precambrian granites (Fig. 5)? The best example is the Vishnu Schist in the Grand Canyon that contains many more radiohalos per slide than either the Ruby Granodiorite or Zoroaster Granite that were previously intruded in it (Ilg et al. 1996; Karlstrom et al. 2003) (Tables 1 and 2). The answer would be that the Vishnu Schist consists of many more biotite grains than in either of those two granites, so the Vishnu Schist has many more perspective ^{238}U-bearing zircon inclusions within those many more sheeted biotite grains which are conducive to fluid flow between the sheets to transport Po and thus generate more Po radiohalos.

D. The Flood/post-Flood boundary

Given the process of radiohalos formation in granites, whereby at least 100 million years' worth of accelerated ^{238}U decay (at today's measured rate) is needed to form good visible radiohalos, it is difficult to draw any conclusions from the radiohalos frequency data plotted in Fig. 6 regarding the location of the Flood/post-Flood boundary in the rock record. That is because there is insufficient "geologic" time left in the Cenozoic (only 66 million years) for the accumulation of enough α-particles from ^{238}U and Po decay to have generated many good visible radiohalos. However, there was still one sampled Cenozoic granite that contained radiohalos, especially Po radiohalos, and is conventionally dated at Oligocene (c. 33 Ma), whereas the other Cenozoic granites contained no radiohalos (Table 1 and Fig. 6).

Two main scenarios have been suggested for the boundary in the rock record that represents the Flood/post-Flood boundary, and each scenario has an accompanying implication for when the accelerated radioactive decay decelerated. The first scenario is that the Flood/post-Flood boundary corresponds roughly with the Cenozoic or Paleogene/Cretaceous boundary at 66 Ma in the rock record (Austin et al 1994; Whitmore and Garner 2008). This scenario involves the continuation of accelerated radioactive decay during the ensuing Cenozoic, though perhaps it began to progressively decelerate. The second scenario places the Flood/post-Flood boundary at or close below the Quaternary/Neogene boundary or alternatively the Pliocene/Miocene boundary in the rock record at approximately 3 Ma or 5-7 Ma (Clarey 2020). Accelerated radioactive decay would likewise have continued through the Cenozoic before decelerating at the end of the Cenozoic. The second scenario is attractive to many as it avoids the harmful bi-products of accelerated radioactive decay (heat and radiation) in the post-Flood era, especially for humans, animals, and plants.

Since both scenarios involve accelerated radioactive decay continuing through the Cenozoic, the radiohalos frequency data plotted in Fig. 6 do not allow any definitive demarcation of the Flood/post-Flood boundary in the rock record. All the data show is they are consistent with the drop-off in radiohalos frequency at and below approximately 80 Ma due to the 100 million years' worth of accelerated ^{238}U decay

(at today's measured rate) being required to generate good visible radiohalos.

VI. CONCLUSIONS

As a physical record of radioactive decay that occurred in granites and metamorphic rocks through earth history radiohalos potentially provide clues as to when the accelerated ^{238}U decay occurred within the Biblical framework of earth history, the demarcation of the pre-Flood/Flood and Flood/post-Flood boundaries in the rock record, and the activity of hydrothermal fluids during the Flood. The occurrence and frequency of radiohalos data was selected for some 147 granites and regional metamorphic rocks spanning the conventional geologic timescale from 33-3200 Ma whose samples followed a protocol of similar numbers of slides scanned for radiohalos per sample averaged accordingly so as to provide statistically robust comparisons between rock units.

The following conclusions were derived from interpretation of the plotted results of radiohalos frequency versus conventional geologic age for the sampled rock units:

(1) The plotted radiohalos frequencies only record the episode of five-orders-of-magnitude accelerated ^{238}U decay that occurred during the Flood as heat generated by that accelerated decay would likely have annealed any previously-generated radiohalos in pre-Flood rocks.

(2) The plotted radiohalos frequency data are consistent with the pre-Flood/Flood boundary being approximately at the Precambrian/Cambrian boundary in the rock record.

(3) The three small peaks in the radiohalos frequencies in Precambrian granites and metamorphic rocks may coincide with the grossly accelerated tectonic activity of God's supernatural creative work on Days 1, 2 and 3 of the Creation Week.

(4) The highest peak in the radiohalos frequency data in the first half of the Phanerozoic coincides with the formation of granites and regional metamorphic rocks during the catastrophic plate tectonics of the Flood.

(5) The radiohalos frequencies are also related to the differing amounts of hydrothermal fluid activity in all the various granites and regional metamorphic rocks during the Flood

(6) Some of the highest radiohalos numbers are in granites associated with hydrothermal metallic ore veins consistent with the highest radiohalos numbers being indicative of hydrothermal fluid activity.

(7) The reason that there are relatively higher radiohalos numbers in some Precambrian regional metamorphic rocks compared to the Precambrian granites may be due to more biotite grains being in those rocks facilitating the generation of many new radiohalos during the Flood as heat from accelerated ^{238}U decay activated water more easily permeating those biotite flakes.

(8) The radiohalos frequency data are unable to distinguish the location of the Flood/post-Flood boundary in the geologic record as 100 million years' worth of accelerated ^{238}U decay (at today's measured rate) are needed to generate good visible radiohalos.

While more samples providing more radiohalos frequency data would infill blank spaces in the spread of data across the geologic timescale and rock record, it is unlikely that these conclusions will be significantly changed. On the hand, further data may enhance and/or add to these conclusions. Thus, further work is encouraged.

ACKNOWLEDGEMENTS

Many willing people gave various assistance over many years to obtain these radiohalos data. Michael Oard, Peter Klevberg, Kurt Wise, Paul Garner, Peter Salkeld, Tom Vail, Dallel Gates, Larry Vardiman, Lior Regev, Darry Stansbury, Richard Bruce, John Whitmore, Ken Lawson, Jaemon Lee, Danny Faulkner, and members of my family either collected and submitted samples, or assisted with the necessary fieldwork. Mark Armitage is especially thanked for his painstaking work in preparing many slides over many years, and for meticulously scanning those slides to identify, count and tabulate the radiohalos, although a few samples were either processed by Dallel Gates and Sara Whitmore or by myself. However, I take full responsibility for the final tabulation of the radiohalos data here, and for plotting and interpreting the results.

REFERENCES

Armitage, M.H., and A.A. Snelling. 2008. Radiohalos and diamonds: Are diamonds really for ever? In A. A. Snelling (editor), *Proceedings of the Sixth International Conference on Creationism*, pp. 323–334. Pittsburgh, Pennsylvania: Creation Science Fellowship; Dallas, Texas: Institute for Creation Research.

Ashley, P.M., N.D.J. Cook, R.L. Hill, and A.J.R. Kent. 1994. Shoshonitic lamprophyre dykes and their relation to mesothermal Au-Sb veins at Hillgrove, New South Wales, Australia. *Lithos* 32:249-272.

Ashley, P.M., and D. Craw. 2004. Structural controls on hydrothermal alteration and gold-antimony mineralization in the Hillgrove area, NSW, Australia. *Mineralium Deposita* 39:223-239.

Audétat, A., D. Günther, and C.A. Heinrich. 2000a. Causes of large-scale metal zonation around mineralized plutons: Fluid inclusion LA-ICP-MS evidence from the Mole Granite, Australia. *Economic Geology* 95:1563-1581.

Audétat, A., D. Günther, and C.A. Heinrich. 2000b. Magmatic-hydrothermal evolution in a fractionating granite: A microchemical study of the Sn-W-F-mineralized Mole Granite (Australia). *Geochimica et Cosmochimica Acta* 64:3373-3393.

Austin, S.A., and K.P. Wise. 1994. The pre-Flood/Flood boundary: As defined in Grand Canyon and East Mojave. In R.E. Walsh (editor), *Proceedings of the Third International Conference on Creationism*, pp.37-47. Pittsburgh, Pennsylvania: Creation Science Fellowship.

Austin, S.A., J.R. Baumgardner, D.R. Humphreys, A. A. Snelling, L. Vardiman, and K.P. Wise. 1994. Catastrophic plate tectonics: A global Flood model of earth history. In R.E. Walsh (editor), *Proceedings of the Third International Conference on Creationism*, pp.609-621. Pittsburgh, Pennsylvania: Creation Science Fellowship.

Bagnall, K.W. 1957. *Chemistry of the Rare Radioelements*. London, UK: Butterworths.

Bain, J.H.C., and J.J. Draper (compilers). 1997. *North Queensland Geology*. Canberra, Australia: Australian Geological Survey Organization; Brisbane, Australia: Geological Survey of Queensland. *AGSO Bulletin* 240.

Bateman, P.C., and B.W. Chappell. 1979. Crystallization, fractionation, and solidification of the Tuolumne Intrusive Series, Yosemite National Park, California. *Geological Society of America Bulletin* 90:465–482.

Baumgardner, J.R. 2000. Distribution of radioactive isotopes in the earth. In L. Vardiman, A.A. Snelling, and E.F. Chaffin (editors), *Radioisotopes and the Age of the Earth: A Young-Earth Creationist Research Initiative*, pp. 49-94. El Cajon, California: Institute for Creation Research; St Joseph, Missouri: Creation Research Society.

Baumgardner, J.R. 2003. Catastrophic plate tectonics: The physics behind

the Genesis Flood. In R.L. Ivey, Jr. (editor), *Proceedings of the Fifth International Conference on Creationism*, pp.113–126. Pittsburgh, Pennsylvania: Creation Science Fellowship.

Bower, W.R., R.A.D. Pattrick, C.I. Pearce, G.T.R. Droop, and S.J. Haigh. 2016a. Radiation damage haloes in biotite investigated using high-resolution transmission electron microscopy. *American Mineralogist* 101:105-110.

Bower, W.R., C.I. Pearce, A.D. Smith, S.M. Plimblott, J.F.W. Mosselmans, S.J. Haigh, J.P. McKinley, and R.A.D. Pattrick. 2016b. Radiation damage in biotite mica by accelerated α-particles: A synchrotron microfocus X-ray diffraction and X-ray absorption spectroscopy study. *American Mineralogist* 101:928-942.

Clarey, T.L. 2020. *Carved in Stone: Geological Evidence of the Worldwide Flood.* Dallas, Texas: Institute for Creation Research.

Comsti, E.C., and G.R. Taylor. 1984. Implications of fluid inclusion data on the origin of the Hillgrove gold-antimony deposits, N.S.W. *Proceedings of the Australasian Institute of Mining and Metallurgy* 289:195-203.

Condie, K.C., E. Belousova, W.L. Griffin, and K.N. Sircombe. 2009. Granitoid events in space and time: Constraints from igneous and detrital zircon age spectra. *Gondwana Research* 15:228–242.

Day, R.W., W.G. Whitaker, C.G. Murray, I.H. Wilson, and K.G. Grimes. 1983. *Queensland Geology: A Companion Volume to the 1:2,500,000 Scale Geological Map (1975).* Brisbane, Australia: Geological Survey of Queensland. *Geological Survey of Queensland Publication* 383.

Dickens, H., and A.A. Snelling. 2008. Precambrian geology and the Bible: A harmony. *Journal of Creation* 22, no. 1:65–72.

Dickens, H. 2018. North American Precambrian geology–A proposed young earth biblical model. In J.H. Whitmore (editor), *Proceedings of the Eighth International Conference on Creationism*, pp. 389–403. Pittsburgh, Pennsylvania: Creation Science Fellowship.

Fremlin, J.H. 1975. Spectacle haloes. *Nature* 258:269.

Gentry, R.V. 1967. Extinct radioactivity and the discovery of a new pleochroic halo. *Nature* 213:487-489.

Gentry, R.V. 1968. Fossil alpha-recoil analysis of certain variant radioactive haloes. *Science* 160:1228-1230.

Gentry, R.V. 1970. Giant radioactive halos: Indicators of unknown radioactivity. *Science* 169:670-673.

Gentry, R.V. 1971. Radiohalos: Some unique lead isotopic ratios and unknown alpha activity. Science 173:727-731.

Gentry, R.V. 1973. Radioactive halos. *Annual Review of Nuclear Science* 23:347-362.

Gentry, R.V., S.S. Christy, J.F. McLaughlin, and J.A. McHugh. 1973. Ion microprobe confirmation of Pb isotope ratios and search for isomer precursors in polonium radiohalos. *Nature* 244:282-283.

Gentry, R.V. 1974. Radiohalos in a radiochronological and cosmological perspective. *Science* 184:62-66.

Gentry, R.V., L.D. Hulett, S.S. Christy, J.F. McLaughlin, J.A. McHugh, and M. Bayard. 1974. "Spectacle" array of ^{210}Po halo radiocentres in biotite: a nuclear geophysical enigma. *Nature* 252:564-566.

Gentry, R.V. 1975. Spectacle haloes. *Nature* 258:269-270.

Gentry, R.V., T.A. Cahill, N.R. Fletcher, H.C. Kaufmann, L.R. Medsker, J.W. Nelson, and R.G. Flocchini. 1976a. Evidence for primordial superheavy elements. *Physical Review Letters* 37, no. 1:11-15.

Gentry, R.V., W.H. Christie, D.H. Smith, J.W. Boyle, S.S. Christy, and J.F. McLaughlin. 1978. Implications on unknown radioactivity of giant and dwarf haloes in Scandinavian rocks. *Nature* 274:457-459.

Gentry, R.V. 1979. Time: Measured responses. *EOS, Transactions of the American Geophysical Union* 60, no. 22:474.

Gentry, R.V. 1980. Polonium halos. *EOS, Transactions of the American Geophysical Union* 61, no. 27:514.

Gentry, R.V. 1982. Creationism again. *Physics Today* 35, no. 10:13.

Gentry, R.V. 1983. Creationism still again. *Physics Today* 36, no. 14:13-15.

Gentry, R.V. 1984. Radioactive haloes in a radiochronological and cosmological perspective. In *Proceedings of the 63rd Annual Meeting, Pacific Division, American Association for the Advancement of Science* 1, no. 3:38-65.

Gentry, R.V. 1986. Radioactive haloes: Implications for creation. In R.E. Walsh, C.L. Brooks, and R.S. Crowell (editors), *Proceedings of the First International Conference on Creationism*, vol. 2, pp. 89-100. Pittsburgh, Pennsylvania: Creation Science Fellowship.

Gentry, R.V. 1988. *Creation's Tiny Mystery*. Knoxville, Tennessee: Earth Science Associates.

Gentry, R.V. 1989. Response to Wise. *Creation Research Society Quarterly* 25:176-180.

Gentry, R.V. 1998. Radiohalos in diamonds. *Creation Ex Nihilo Technical Journal* 12:287-290.

Glazner, A.F., and B.R. Johnson. 2013. Late crystallization of K-feldspar and the paradox of megacrystic granites. *Contributions to Mineralogy and Petrology* 166:777-779.

Glazner, A.F., V.R. Baker, J.M. Bartley, K.M. Bohacs, and D.R. Coleman. 2022. The rocks don't lie, but they can be misunderstood. *Geology Today* 32, no.10:4-10.

Harada, K., W.C. Burnett, P.A. LaRock, and J.B. Cowart. 1989. Polonium in Florida groundwater and its possible relationship to the sulfur cycle and bacteria. *Geochimica et Cosmochimica Acta* 53:143-150.

Henderson, G.H., and S. Bateson. 1934. A quantitative study of pleochroic haloes – I. *Proceedings of the Royal Society of London, Series A* 145:563-581.

Henderson, G.H., and L.G. Turnbull. 1934. A quantitative study of pleochroic haloes – II. *Proceedings of the Royal Society of London, Series A* 145:582-598.

Henderson, G.H., G.M. Mushkat, and D.P. Crawford. 1934. A quantitative study of pleochroic haloes – III. Thorium. *Proceedings of the Royal Society of London, Series A* 158:199-211.

Henderson, G.H., and F.W. Sparks. 1939. A quantitative study of pleochroic haloes – IV. New types of haloes. *Proceedings of the Royal Society of London, Series A* 173:238-249.

Henderson, G.H. 1939. A quantitative study of pleochroic haloes – V. The genesis of haloes. *Proceedings of the Royal Society of London, Series A* 173:250-264.

Holmes, A. 1931. Radioactivity and geological time. *Bulletin of the National Research Council* 80:124-460.

Humphreys, D.R. 2000. Accelerated nuclear decay: A viable hypothesis? In L. Vardiman, A.A. Snelling, and E.F. Chaffin (editors), *Radioisotopes and the Age of the Earth: A Young-Earth Creationist Research Initiative*, pp. 333-379. El Cajon, California: Institute for Creation Research; St Joseph, Missouri: Creation Research Society.

Hussain, N., T.M. Church, G.W. Luther III, and W.S. Moore. 1995. ^{210}Po and ^{210}Pb disequilibrium in the hydrothermal vent fluids in chimney deposits from Juan de Fuca Ridge. *Geophysical Research Letters* 22:3175-3178.

Iimori, S., and J. Yoshimura. 1926. Pleochroic halos in biotite: Probable existence of the independent origin of the actinium series. *Scientific Papers of the Institute of Physical and Chemical Research* 5, no. 66:11-24.

Ilg, B.R., K.E. Karlstrom, D.P. Hawkins, and M.L. Williams. 1996. Tectonic evolution of Paleoproterozoic rocks in the Grand Canyon: Insights into middle-crustal processes. *Geological Society of America Bulletin* 108, no. 9:1149-1166.

Joly, J. 1907. Pleochroic halos. *Philosophical Magazine* 13:381-383.

Joly, J. 1917a. Radio-active halos. *Philosophical Transactions of the Royal Society of London, Series A* 217:51-79.

Joly, J. 1917b. Radio-active halos. *Nature* 99:456-458, 476-478.

Joly, J. 1923. Radio-active halos. *Proceedings of the Royal Society of London, Series A* 102:682-705.

Joly, J. 1924. The radioactivity of the rocks. *Nature* 114:160-164.

Karlstrom, K.E., B.R. Ilg, M.L. Williams, D.P. Hawkins, S.A. Bowring, and S.J. Seaman. 2003. Paleoproterozoic rocks of the Granite Gorges. In S.S. Beus and M. Morales (editors), *Grand Canyon Geology*, second edition, pp. 9-38. New York, USA: Oxford University Press.

Kerr-Lawson, D.E. 1927. Pleochroic haloes in biotite from near Murray Bay. *University of Toronto Studies in Geology Series* 24:54-71.

Kerr-Lawson, D.E. 1928. Pleochroic haloes in biotite. *University of Toronto Studies in Geology Series* 27:15-27.

Kleeman, J.D., I.R. Plimer, J. Lu, D.A. Foster, and R. Davidson. 1997. Timing of thermal and mineralization events associated with the Mole Granite, New South Wales. *Geological Society of Australia Special Publication* 19:254-265.

Laney, R., and A.W. Laughlin. 1981. Natural annealing of the pleochroic haloes in biotite samples from deep drill holes, Fenton Hill, New Mexico. *Geophysical Research Letters* 8, no.5:501-504.

LaRock, P.A., J.-H. Hyun, S. Boutelle, W.C. Burnett, and C.D. Hull. 1996. Bacterial mobilization of polonium. *Geochimica et Cosmochimica Acta* 60:4321-4328.

LeCloarec, M.F., M. Pennisi, E. Corazza, and G. Lambert. 1994. Origin of fumerolic fluids emitted from a nonerupting volcano: Radionuclide constraints at Vulcano (Aeolian Islands, Italy). *Geochimica et Cosmochimica Acta* 58:4401-4410.

Lingen, J.S., van der. 1926. Ueber pleochroitische höfe. *Zentralel. Mineralogie und Geologie, Abteilung A*. 177-183.

Moscati, R.J., and L.A. Neymark. 2020. U–Pb geochronology of tin deposits associated with the Cornubian Batholith of southwest England: Direct dating of cassiterite by in situ LA-ICPMS. *Mineralium Deposita* 55:1-20.

Mügge, O. 1907. Radioaktivität als ursuche der pleochroitischen höfe des cordierite. *Zentralel. Mineralogie und Geologie* 1907:397-399.

Nance, R.D., J.B. Murphy, and M. Santosh. 2014. The supercontinent cycle: A retrospective essay. *Gondwana Research* 25:4-29.

Peters, S.E., and R.R. Gaines. 2012. Formation of the "Great Unconformity" as a trigger for the Cambrian explosion. *Nature* 484:363-366.

Ramdohr, P. 1933. *Neues Jahrbuch für Mineralogie Beilageband Abteilung A* 67:53-65.

Ramdohr, P. 1957. *Abh. Deut. Akad. Wiss. Berlin Kl. Chem. Geol. Biol*. 2:1-17.

Ramdohr, P. 1960. Neue beobachtungen an Radioacktiven Höfen in verschiedenen Mineralien mit kritischen bemerkungen zur auswertung der Höfe zur Altersbestimmung. *Geologische Rundschau* 49:253-263.

Rubin, K. 1997. Degassing of metals and metalloids from erupting seamount and mid-ocean ridge volcanoes: Observations and predictions. *Geochimica et Cosmochimica Acta* 61:3525-3542.

Schaltegger, U., T. Pettke, A. Audétat, E. Reusser, and C.A. Heinrich. 2000. Magmatic-to-hydrothermal crystallization in the W-Sn mineralized Mole Granite (NSW, Australia) Part I: Crystallization of zircon and REE-phosphates over three million years – a geochemical and U-Pb geochronological study. *Chemical Geology* 220:215-235.

Schilling, A. 1926. Die radioacktiven höfe im flusspat von Wölsendorf. *Neues Jahrbuch für Mineralogie, Geologie und Palaeontology, Abteilung A* 53:241-265.

Schulze, D.J., and L. Nasdala. 2017. Unusual paired pattern of radiohaloes on a diamond crystal from Guaniamo (Venezuela). *Lithos* 265:177-181.

Snelling, A.A., and J. Woodmorappe. 1998. The cooling of thick igneous bodies on a young earth. In R.E. Walsh (editor), *Proceedings of the Fourth International Conference on Creationism*, pp. 527-545. Pittsburgh, Pennsylvania: Creation Science Fellowship.

Snelling, A.A. 2000a. Geochemical processes in the mantle and crust. In L. Vardiman, A.A. Snelling, and E.F. Chaffin (editors), *Radioisotopes and the Age of the Earth: A Young-Earth Creationist Research Initiative*, pp. 123-304. El Cajon, California: Institute for Creation Research; St. Joseph, Missouri: Creation Research Society.

Snelling, A.A. 2000b. Radiohalos. In L. Vardiman, A.A. Snelling, and E.F. Chaffin (editors), *Radioisotopes and the Age of the Earth: A Young-Earth Creationist Research Initiative*, pp. 381-468. El Cajon, California: Institute for Creation Research; St. Joseph, Missouri: Creation Research Society.

Snelling, A.A., and M.H. Armitage. 2003. Radiohalos – A tale of three granitic plutons. In R.L. Ivey, Jr. (editor), *Proceedings of the Fifth International Conference on Creationism*, pp. 243-267. Pittsburgh, Pennsylvania: Creation Science Fellowship.

Snelling, A.A., J.R. Baumgardner, and L. Vardiman. 2003. Abundant Po radiohalos in Phanerozoic granites and timescale implications for their formation. *EOS, Transactions of the American Geophysical Union* 84, no. 46, Fall Meeting Supplement: Abstract V32C-1046.

Snelling, A.A. 2005a. Radiohalos in granites: Evidence of accelerated nuclear decay. In L. Vardiman, A.A. Snelling, and E.F. Chaffin (editors), *Radioisotopes and the Age of the Earth: Results of a Young-Earth Creationist Research Initiative*, pp. 101-207. El Cajon, California: Institute for Creation Research; Chino Valley, Arizona: Creation Research Society.

Snelling, A.A. 2005b. Fission tracks in zircons: Evidence of abundant nuclear decay. In L. Vardiman, A.A. Snelling, and E.F. Chaffin (editors), *Radioisotopes and the Age of the Earth: Results of a Young-Earth Creationist Research Initiative*, pp. 209-324. El Cajon, California: Institute for Creation Research; Chino Valley, Arizona: Creation Research Society.

Snelling, A.A. 2005c. Isochron discordances and the role of inheritance and mixing of radioisotopes in the mantle and crust. In L. Vardiman, A.A. Snelling, and E.F. Chaffin (editors), *Radioisotopes and the Age of the Earth: Results of a Young-Earth Creationist Research Initiative*, pp. 393-524. El Cajon, California: Institute for Creation Research; Chino Valley, Arizona: Creation Research Society.

Snelling, A.A. 2008a. Catastrophic granite formation: Rapid melting of source rocks, and rapid magma intrusion and cooling. *Answers Research Journal* 1:11–25.

Snelling, A.A. 2008b. Testing the hydrothermal fluid transport model for polonium radiohalo formation: The Thunderhead Sandstone, Great Smoky Mountains, Tennessee-North Carolina. *Answers Research Journal* 1:53-64.

Snelling, A. A. 2008c. Radiohalos in the Cooma Metamorphic Complex, New South Wales, Australia: The mode and rate of regional metamorphism. In A.A. Snelling (editor), *Proceedings of the Sixth International Conference on Creationism*, pp.371-387. Pittsburgh, Pennsylvania: Creation Science Fellowship; Dallas, Texas: Institute for Creation Research.

Snelling, A.A. 2008d. Radiohalos in the Shap Granite, Lake District, England: Evidence that removes objections to Flood geology. In A. A. Snelling (editor), *Proceedings of the Sixth International Conference on Creationism*, pp. 389–405. Pittsburgh, Pennsylvania: Creation Science Fellowship; Dallas, Texas: Institute for Creation Research.

Snelling, A.A., and D. Gates. 2009. Implications of polonium radiohalos in nested plutons of the Tuolumne Intrusive Suite, Yosemite, California. *Answers Research Journal* 2:53-77.

Snelling, A.A. 2009. *Earth's Catastrophic Past: Geology, Creation, and the Flood*. Dallas, Texas: Institute for Creation Research.

Snelling, A.A. 2014. Radiohalos in multiple, sequentially intruded phases of the Bathurst Batholith, NSW, Australia: Evidence for rapid granite formation during the Flood. *Answers Research Journal* 7:49-81.

Snelling, A.A. 2018. Radiohalos as an exploration pathfinder for granite-re-

lated hydrothermal ore veins: A case study in the New England Batholith, Eastern Australia. In J.H. Whitmore (editor), *Proceedings of the Eighth International Conference on Creationism*, pp. 567–580. Pittsburgh, Pennsylvania: Creation Science Fellowship.

Snelling, A.A. 2022. The Genesis Flood Revisited. Green Forest, Arkansas: Master Books; Hebron, Kentucky: Answers in Genesis.

Stark, M. 1936. Pleochroitische (radioacktive) höfe ihre verbreitung in den gesteinen und veränderlickheit. *Chemie der Erde* 10:566-630.

Stevens, B.P.J., and G.M. Bradley. 2018. Sedimentology in metamorphic rocks, the Willyama Supergroup, Broken Hill, Australia. *Australian Journal of Earth Sciences* 65, no. 1:25-59.

Vardiman, L., A.A. Snelling, and E.F. Chaffin (editors). 2005. *Radioisotopes and the Age of the Earth: Results of a Young-Earth Creationist Research Initiative*. El Cajon, California: Institute for Creation Research; Chino Valley, Arizona: Creation Research Society.

Voice, P.J., M. Kowalewski, and K.A. Eriksson. 2011. Quantifying the timing and rate of crustal evolution: Global compilation of radiometrically dated detrital zircon grains. *The Journal of Geology* 119, no. 2:109–126.

Whitmore, J.H., and P.A. Garner. 2008. Using suites of criteria to recognize pre-Flood, Flood, and post-Flood strata in the rock record with application to Wyoming (USA). In A.A. Snelling (editor), *Proceedings of the Sixth International Conference on Creationism*, pp. 425–448. Pittsburgh, Pennsylvania: Creation Science Fellowship; Dallas, Texas: Institute for Creation Research.

Wiman, E. 1930. Studies of some Archaean rocks in the neighbourhood of Uppsala, Sweden, and of their geological position. *Bulletin of the Geological Institute, University of Uppsala* 23:1-170.

Wise, K.P. 1989. Radioactive halos: Geological concerns. *Creation Research Society Quarterly* 25:171-176.

THE AUTHOR

Andrew A. Snelling obtained a PhD in geology from the University of Sydney, Australia, then worked a few years in the exploration and mining industry and in mineral deposit research, before working in full-time creation ministry and research since late 1983, first with the Australian ministry, then with the Institute for Creation Research, and now with Answers in Genesis (USA). He was the founding editor of what is now the *Journal of Creation*, was involved in the RATE project as a principal researcher and editor, was the 6th ICC editor, and is founding editor of the *Answers Research Journal.*